Chapter 7
Metallic Nanostructures for Electrocatalysis

Zhenmeng Peng

Abstract The metal electrocatalyst research requires molecular-level knowledge of the electrocatalytic reactions and the controlling factors that determine the reaction kinetics. Several important factors, including electronic structure and geometric structure of metal surfaces, third-body effect, and bifunctional effect, are discussed for their roles in electrocatalysis. Chemical stability and surface restructuring/segregation of metals, which need practical consideration in the electrocatalyst research, are introduced. The electrochemistry of oxygen, hydrogen, carbon-containing compounds, and nitrogen-containing compounds is reviewed. Discussions are focused on recent advances in preparing metallic nanostructures for these reactions, and on understanding the relationship between the physical parameters of metallic nanostructures and the electrocatalytic property.

7.1 Introduction

Metallic nanostructures for electrocatalysis have been an area of active research for decades and can find important applications in many research areas and industries [1–6], including energy generation, chemicals production, electrochemical sensors, environmental control, and so on. With increasing concerns over environments and depletion of fossil fuels in recent years, more research efforts have been put into utilizing alternative energy resources and developing clean energy technologies. For example, polymer electrolyte membrane fuel cells (PEMFCs), which can generate electric energy by electrochemically reacting hydrogen and oxygen, have been researched for automobiles [7–11]. Metal–air batteries have been developed to improve the power density and efficiency of portable energy devices [12–15]. Electrochemical water splitting has been recently considered as a clean and alternative technology for producing H_2 [16–18], which is both energy carrier and important

Book Chapter to "Metallic Nanostructures: form Controlled Synthesis to Applications"

Z. Peng (✉)
Department of Chemical and Biomolecular Engineering, University of Akron,
Akron, OH 44325, USA
e-mail: zpeng@uakron.edu

Y. Xiong, X. Lu (eds.), *Metallic Nanostructures,* DOI 10.1007/978-3-319-11304-3_7

chemical commodity. All these technologies involve electrochemical reactions and require the use of metallic nanostructures for promoting the reaction kinetics. Research of metallic nanostructures as efficient electrocatalyst thus becomes crucial to advance these energy technologies.

Metal electrocatalyst researches in the early years have once been highly empirical, primarily based on trial-and-error experiments and research experiences. It was caused by the fact that electrocatalysis is governed by multiple parameters of both reaction and catalyst and that these parameters often intervene with each other to affect the catalytic property. With rapid advances in both experimental and theoretical tools nowadays, electrocatalytical reactions can be better understood at molecular level. Many theories have also been proposed to guide metal electrocatalyst research and development. In this chapter, we will first introduce the fundamentals for metal electrocatalysis and electrocatalyst, and then discuss recent examples of metallic nanostructures for electrocatalysis.

7.2 Electrochemical Reaction

7.2.1 Thermodynamics of Electrochemical Reaction

An electrochemical reaction involves the transfer of electrons between two substances: one, a solid (electrode), and the other, a liquid (electrolyte) in most cases. In principle, every redox chemical reaction, $aA + bB \rightarrow cC + dD$, can be written into two electrochemical reactions, in which one gains the electrons being generated from the other [19]:

$$aA \rightarrow cC + ne^- \tag{7.1}$$

$$bB + ne^- \rightarrow dD \tag{7.2}$$

An electrochemical cell can be built by separating occurrence of the two electrochemical reactions at different electrodes and connecting the electrodes using electrolyte and an external circuit (Fig. 7.1). Thus, the electrochemical reactions are also called half-cell reactions. One major difference between a redox chemical reaction and an electrochemical cell made of the reaction is their energy conversion. A redox chemical reaction releases/absorbs thermal energy during the course of reaction, whereas an electrochemical cell generates/consumes electric energy. The open-circuit voltage of the cell (E_{cell}) can be correlated with the Gibbs free energy change of the reaction (ΔG) using the following equation:

$$\Delta G = -nFE_{cell} \tag{7.3}$$

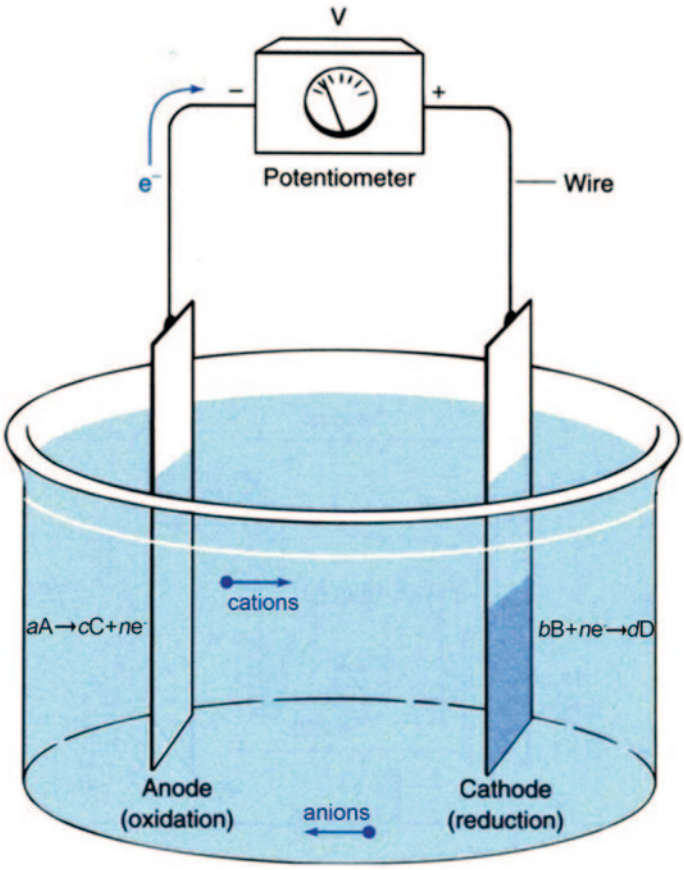

Fig. 7.1 An electrochemical cell constructed using redox chemical reaction $aA + bB \rightarrow cC + dD$

where F is the Faraday constant and has a value of 96485 C/mol. An electrochemical cell made of spontaneous redox chemical reactions (negative ΔG) has a positive E_{cell} and is often called galvanic cell. It can be utilized to convert chemical energy stored in fuel molecules into electric energy. On the other hand, one made of nonspontaneous redox reactions (positive ΔG) is called electrolytic cell and can be utilized to produce valuable chemicals by inputting electric energy into the reaction system. One example is the reaction between H_2 and O_2, which is a spontaneous redox reaction [20]:

$$2H_2 + O_2 \rightarrow 2H_2O \quad (\Delta G^0 = -475 \text{ KJ/mol}) \tag{7.4}$$

A PEMFC can be constructed by separating H_2 oxidation and O_2 reduction at anode and cathode, having a PEM in between, and connecting the electrodes with an electric circuit. The two half-cell reactions can be depicted as follows:

Table 7.1 Standard redox potentials of half-cell reactions

Half-cell reaction	$E^0_{C/A}$ (V vs. SHE)
$N_2 + 6H_2O + 6e^- \Leftrightarrow 2NH_3 + 6OH^-$	−0.77
$N_2 + 4H^+ + 4e^- \Leftrightarrow N_2H_4$	−0.39
$CO_2 + 2H^+ + 2e^- \Leftrightarrow HCOOH$	−0.25
$CO_2 + 2H^+ + 2e^- \Leftrightarrow CO + H_2O$	−0.10
$2H^+ + 2e^- \Leftrightarrow H_2$	0.00
$CO_2 + 6H^+ + 6e^- \Leftrightarrow CH_3OH + H_2O$	0.04
$CO_2 + 12H^+ + 12e^- \Leftrightarrow CH_3CH_2OH + 3H_2O$	0.08
$O_2 + 2H_2O + 4e^- \Leftrightarrow 4OH^-$	0.401
$O_2 + 2H^+ + 2e^- \Leftrightarrow H_2O_2$	0.695
$O_2 + 4H^+ + 4e^- \Leftrightarrow 2H_2O$	1.229

$$2H_2 \rightarrow 4H^+ + 4e^- \tag{7.5}$$

$$O_2 + 4H^+ + 4e^- \rightarrow 2H_2O \tag{7.6}$$

H_2 is electrochemically oxidized into protons because of its higher susceptibility to lose electrons than O_2. O_2 gains the electrons from H_2 electro-oxidation and is reduced into H_2O. Such a PEMFC has an open-circuit cell voltage of $E^0_{cell} = 1.229$ V if being operated under the standard condition.

Redox potentials are defined for half-cell reactions to represent their ability to gain or lose electrons electrochemically. The voltage of cells constructed using any two half-cell reactions can thus be described using the following equation:

$$E_{cell} = E_{cathode} - E_{anode} \tag{7.7}$$

The redox potentials are not absolute values, but rather relative ones comparing to reference electrode reactions. One most often used reference is the standard hydrogen electrode (SHE), which operates under the standard condition and has a defined redox potential of $E^0_{H^+/H_2} = 0$V. By constructing an electrochemical cell using any given half-cell reaction and the SHE and measuring the cell voltage, its redox potential vs. SHE can be determined using the following equation:

$$E_{C/A} = E^0_{cell} + E^0_{H^+/H_2} = E^0_{cell} \tag{7.8}$$

Table 7.1 lists a few half-cell reactions of electrocatalysis importance and their equilibrium redox potentials under standard condition ($E^0_{C/A}$). The redox potential under nonstandard conditions can be calculated using the Nernst equation:

$$E_{C/A} = E^0_{C/A} - \frac{RT}{nF} ln \frac{[A]^a}{[C]^c} \tag{7.9}$$

Correspondingly, the open-circuit voltage of any electrochemical cell operating under nonstandard conditions can also be calculated:

$$E_{cell} = E^0_{B/D} - E^0_{C/A} \frac{RT}{nF} ln \frac{[C]^c [D]^d}{[A]^a [B]^b} \tag{7.10}$$

7.2.2 Kinetics of Electrochemical Reaction

Many theories have been developed for understanding the kinetics of chemical reaction. In the transition state theory, reactants overcome an energy barrier to generate active intermediates, which further react to form products. The rate constant, k, can be described using the Arrhenius equation [21]:

$$k = Ae^{-E_a/RT} \tag{7.11}$$

where A is a pre-exponential constant, E_a is the activation energy, R is the gas constant, and T is the reaction temperature. For an elementary reaction, the reaction rate is simply the production of k and concentration(s) of the reactant(s). For a complex reaction that contains multiple elementary steps, the reaction kinetics is determined by the rate-limiting step. The rate law is an algebraic function of k, concentration(s) of the reactant(s), and some constant parameters.

The kinetics of electrochemical reactions can also been understood using the transition state theory. Comparing to chemical reactions, electrode potential (E) serves as one additional factor for controlling the electrochemical reaction kinetics. The electrode potential can alter the energy barrier and consequently influence the reaction rate (Fig. 7.2). If we consider an elementary half-cell reaction $O + ne \underset{k_b}{\overset{k_f}{\Leftrightarrow}} R$ and use current density (i) to represent the reaction rate, the relationship between i and E can be depicted using the Butler–Volmer equation [22]:

$$i = i_0 \left[e^{-\alpha nF\eta/RT} - e^{(1-\alpha)nF\eta/RT} \right] \tag{7.12}$$

$$i_0 = nFAk_f^{1-\alpha} k_b^{\alpha} [O]^{1-\alpha} [R]^{\alpha} \tag{7.13}$$

$$\eta = E - E_{O/R} \tag{7.14}$$

where i_0 is the exchange current density, α is the charge transfer coefficient, η is the overpotential, E and $E_{O/R}$ are the electrode potential and redox potential, and k_f and k_b are the rate constant for the forward and reverse half-cell reaction. When η=0,

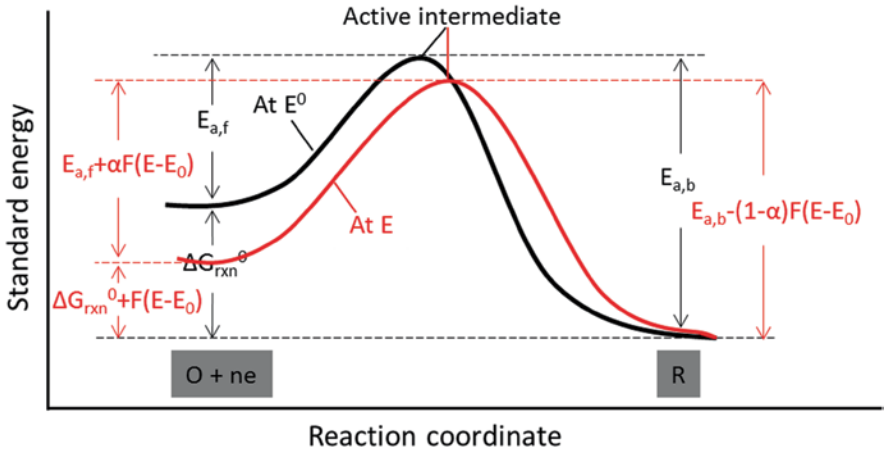

Fig. 7.2 Free energy changes during a reaction and effects of a potential change on the reaction

which represents the electrode stays at the redox potential, i is equal to zero and the half-cell reaction is at its equilibrium. The i value is positive and increases rapidly with η when $E<E_{O/R}$ (negative η), indicating a reduction process. It becomes negative and the value changes exponentially with η when $E>E_{O/R}$ (positive η), corresponding to an oxidation process (Fig. 7.3).

The half-cell reactions can be classified into reversible and irreversible systems based on their intrinsic reaction kinetics. For reversible half-cell reactions, electrons can be rapidly exchanged at the electrode and the i_0 value is relatively large. A small η can lead to a large increase in i (Fig. 7.3). The apparent reaction rate is limited by the diffusion of reacting species rather than the fast reaction kinetics. Cyclic voltammetry of such reactions shows defined distance between peak potentials, and the peak current densities can be calculated using the Randles–Sevcik equation (Fig. 7.4):

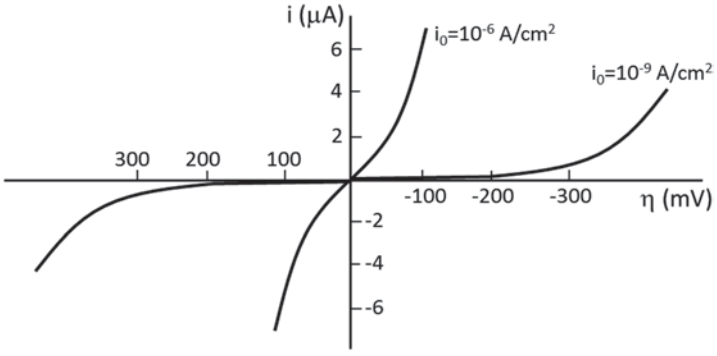

Fig. 7.3 Current density (i) vs. overpotential (μ) curves for the reaction $O+ne\underset{k_r}{\overset{k_f}{\Leftrightarrow}}R$ with different i_0

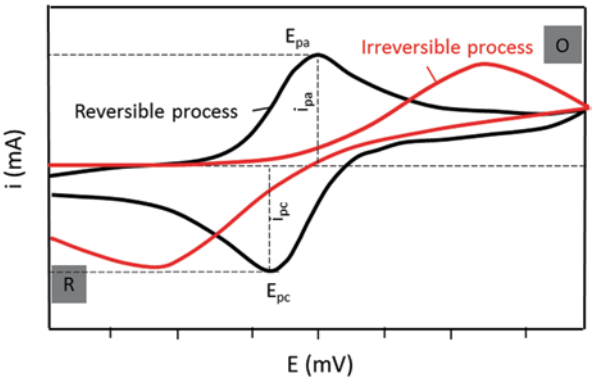

Fig. 7.4 Cyclic voltammetry curves of reversible and irreversible electrochemical processes

$$E_{pa} - E_{pc} = \frac{59}{n} mV \tag{7.15}$$

$$i_p = 2.69 \times 10^8 \times n^{3/2} \times EA \times D^{1/2} \times v^{1/2} \times C \tag{7.16}$$

where E_{pa} and E_{pc} are the anodic and cathodic peak potentials, i_{pc} and i_{pc} are the corresponding peak currents, EA is the electrode area, D is the diffusion coefficient of reacting species, v is the potential scan rate, and C is the concentration of reacting species ([O] for calculating i_{pc} and [R] for calculating i_{pa}).

For irreversible processes (those with sluggish electron exchange and thus small i_0), the two peaks are reduced in size and widely separated when being compared with reversible systems. Totally irreversible systems are characterized by a shift of the peak potential with the scan rate:

$$E_p = E_{O/R} - \frac{RT}{\alpha n_a F}\left[0.78 - ln\left(\frac{k}{D^{1/2}}\right) + ln\left(\frac{\alpha n_a F v}{RT}\right)^{1/2}\right] \tag{7.17}$$

where n_a is the number of electrons involved in the charge-transfer step, k is the rate constant (k_f for calculating E_{pc} and k_b for calculating E_{pa}), and v is scan rate. The peak current density can be given by:

$$i_p = 2.99 \times 10^8 \times n \times (\alpha \times n_a)^{1/2} \times EA \times D^{1/2} \times v^{1/2} \times C \tag{7.18}$$

The i_p value is still proportional to the bulk concentration, but will be lower in height (depending on the value of α).

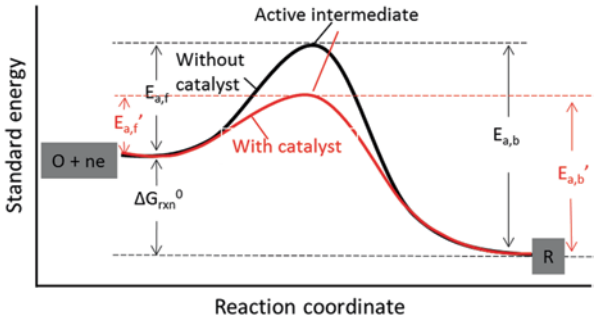

Fig. 7.5 Free energy changes during an electrochemical reaction with and without metal electrocatalysis

7.3 Fundamentals for Metal Electrocatalysis

7.3.1 Mechanism of Metal Electrocatalysis

As being discussed in Chap. 7.2.2, electrochemical reactions can be classified into reversible and irreversible processes based on their exchange current density, i_0. One characteristic of the irreversible processes is a much smaller i_0 and thus the requirement of a much larger η to achieve a same i as for the reversible processes (Eq. 7.12 and Fig. 7.3). If an electrochemical cell is constructed using irreversible half-cell reactions, the working cell voltage will be significantly smaller than the open-circuit value. Consequently, the energy conversion efficiency will be significantly lower than the theoretical value.

The irreversible half-cell reaction kinetics can be improved by metal electrocatalysis. From Eq. 7.13, i_0 is affected by several parameters, including the number of electrons being transferred (n), the pre-exponential constant (A), the charge transfer coefficient (α), the concentration of reacting species ([O] and [R]), and the rate constants (k_f and k_b). k_f and k_b depict the intrinsic kinetics of forward and reverse half-cell reactions. Similar to chemical reactions, k_f and k_b for the half-cell reactions also follow the Arrhenius law (Eq. 7.11) and are functions of their activation energy ($E_{a,f}$ and $E_{a,b}$). The irreversible half-cell reactions have large $E_{a,f}$ and $E_{a,b}$ values, which cause small k_f and k_b. In consequence, a small i_0 is resulted and a large η is required for the half-cell reaction to occur effectively.

Metals can change the reaction rate by promoting a different molecular path for half-cell reactions, which is named metal electrocatalysis. Rather than directly exchanging electrons with electrode, the reacting species first interact with metal surface atoms. The interaction can lead to the generation of altered active intermediates, which further exchange electrons with electrode and react [23]. By altering the reaction path, the energy barrier can be effectively decreased, leading to improved rate constant and thus increased reaction kinetics (Fig. 7.5) [24].

7.3.2 Kinetics of Metal Electrocatalysis

The overall reaction rate of an electrocatalytic reaction is limited by the rate of the slowest step in the path, including diffusion of reactant(s) from bulk electrolyte to catalyst surface, electrocatalytic reaction, and diffusion of product(s) from catalyst surface back to bulk electrolyte. Here we focus on electrocatalysis and assume the diffusions are much faster than the electrocatalytic reaction rate, which means that the concentrations of reacting species on catalyst surface are equal to those in bulk electrolyte and the overall reaction is controlled by metal electrocatalysis. If we consider a simple half-cell reaction $O + ne \underset{k_b}{\overset{k_f}{\Leftrightarrow}} R$ occurring under metal electrocatalysis, the reaction path typically involves three steps including reactant adsorption, surface reaction, and product desorption:

$$O + S \underset{k_{-A}}{\overset{k_A}{\Leftrightarrow}} O \cdot S \tag{7.19}$$

$$O \cdot S + ne \underset{k_{-S}}{\overset{k_S}{\Leftrightarrow}} R \cdot S \tag{7.20}$$

$$R \cdot S \underset{k_{-D}}{\overset{k_D}{\Leftrightarrow}} R + S \tag{7.21}$$

where S stands for metal active sites, and $O{\cdot}S$ and $R{\cdot}S$ are adsorbed O and R species. The overall reaction rate law (r) is determined by the rate-limiting step, which can fall in one of the following three situations for different reactions and/or using different catalysts.

1. Adsorption-limited process:

$$r = \frac{(k_A[O] - k_{-A}K_R[R]/K_S) \cdot C_t}{1 + K_R[R] + K_R[R]/K_S} \tag{7.22}$$

2. Surface reaction-limited process:

$$r = \frac{(k_S K_O[O] - k_{-S}K_R[R]) \cdot C_t}{1 + K_O[O] + K_R[R]} \tag{7.23}$$

3. Desorption-limited process:

$$r = \frac{(k_D K_S K_O[O] - k_{-D}[R]) \cdot C_t}{1 + K_O[O] + K_S K_O[O]} \tag{7.24}$$

where k_A and k_{-A} are the rate constants for [O] adsorption, k_S and k_{-S} are the rate constants for the surface reaction, k_D and k_{-D} are the rate constants for [R] desorption, K_O and K_R are the equilibrium constants for O and R adsorption, K_S is the

equilibrium constant for the surface reaction, and C_t is the concentration of metal active sites. The electrochemical reaction is at equilibrium, i.e. $r=0$, at $\eta=0$.

The exchange current density, i_0, is largely determined by the rate constants of the rate-limiting step from the aforementioned rate law expressions. Taking the surface reaction-limited process as one example, both K_O and K_R are significantly larger in values than k_S and k_{-S}. If we consider a special case where K_O and K_R have similar values and O and R have comparable concentrations, the apparent rate constants for the forward and reverse half-cell reaction under metal electrocatalysis will become $k_f^{'} \approx k_s / 2$ and $k_b^{'} \approx k_{-s} / 2$. In another word, the rate constants for the overall electrochemical reaction are directly determined by the rate constants of the surface reaction step for a surface reaction-limited mechanism. If we take $k_f^{'}$ and $k_b^{'}$ values into Eq. 7.13, we can describe i_0 as a function of k_S and k_{-S}:

$$i_0 \approx nFA(k_S / 2)^{1-\alpha}(k_{-S} / 2)^{\alpha}\left[O\right]^{1-\alpha}\left[R\right]^{\alpha} \tag{7.25}$$

From this equation, the electrochemical reaction kinetics of a surface reaction-limited process can be promoted by using metal catalysts that exhibit high k_S and k_{-S} values.

7.4 Fundamentals for Metal Electrocatalyst

An electrocatalyst by definition is a catalyst that participates in an electrochemical reaction and alters the reaction kinetics without being consumed in the process. Many types of materials can serve as electrocatalyst, among which metals are most often used for their outstanding property. Chapter 7.3 provides discussions on the mechanism of metal electrocatalysis and the kinetics of electrocatalytic reactions. Similar to heterogeneous catalyst, metal electrocatalyst is reaction specific. A metal electrocatalyst good for one electrochemical reaction might be completely inactive for another. For a same electrochemical reaction, some metals exhibit high activity, while some others are inert. For surface sensitive electrochemical reactions, the property of metal electrocatalyst can be significantly altered by the nature of the metal surfaces exposed. From Chaps. 7.2 and 7.3, we learn the electrochemical reaction kinetics is determined by i_0, which can be affected by the interaction between reacting species and metal active sites. In this section, we discuss several major factors that can affect the metal-reacting species interaction and thus the reaction kinetics.

7.4.1 Electronic Effect

As being discussed in Chap 7.3, metal electrocatalysis involves interaction between reacting species and metal active sites. At molecular level, the interaction is caused by the different energy levels of their outer-layer electrons, which lead to electron

Table 7.2 Shifts in d-band centers, ε_d, of surface impurities (A) and overlayers (B) relative to the clean metal values (bold).

	Fe	Co	Ni	Cu	Ru	Rh	Pd	Ag	Ir	Pt	Au
A											
Fe	**−0.92**	−0.05	−0.20	−0.13	−0.29	−0.54	−1.24	−0.83	−0.36	−1.09	−1,42
Co	0.01	**−1.17**	−0.28	−0.16	−0.24	−0.58	−1.37	−0.91	−0.36	−1.19	−1.56
Ni	0.09	0.19	**−1.29**	0.19	−0.14	−0.31	−0.97	−0.53	−0.14	−0.80	−1.13
Cu	0.56	0.60	0.27	**−2.67**	0.58	0.32	−0.64	−0.70	0.58	−0.33	−1.09
Ru	0.21	0.26	0.01	0.12	**−1.41**	−0.17	−0.82	−0.27	0.02	−0.62	−0.84
Rh	0.24	0.34	0.16	0.44	0.04	**−1.73**	−0.54	0.07	0.17	−0.35	−0.49
Pd	0.37	0.54	0.50	0.94	0.24	0.36	**−1.83**	0.59	0.53	0.19	0.17
Ag	0.72	0.84	0.67	0.47	0.84	0.86	0.14	**−4.30**	1.14	0.50	−0.15
Ir	0.21	0.27	0.05	0.21	0.09	−0.15	−0.73	−0.13	**−2.11**	−0.56	−0.74
Pt	0.33	0.48	0.40	0.72	0.14	0.23	−0.17	0.44	0.38	**−2.25**	−0.05
Au	0.63	0.77	0.63	0.55	0.70	0.75	0.17	0.21	0.98	0.46	**−3.56**
B											
Fe	**−0.92**	0.14	−0.04	−0.05	−0.73	−0.72	−1.32	−1.25	−0.95	−1.48	−2.19
Co	−0.01	**−1.17**	−0.20	−0.06	−0.70	−0.95	−1.65	−1.36	−1.09	−1.89	−2.39
Ni	0.96	0.11	**−1.29**	0.12	−0.63	−0.74	−1.32	−1.14	−0.86	−1.53	−2.10
Cu	0.25	0.38	0.18	**−2.67**	−0.22	−0.27	−1.04	−1.21	−0.32	−1.15	−1.96
Ru	0.30	0.37	0.29	0.30	**−1.41**	−0.12	−0.47	−0.40	−0.13	−0.61	−0.86
Rh	0.31	0.41	0.34	0.22	0.03	**−1.73**	−0.39	−0.08	0.03	−0.45	−0.57
Pd	0.36	0.54	0.54	0.80	−0.11	0.25	**−1.83**	0.15	0.31	0.04	−0.14
Ag	0.55	0.74	0.68	0.62	0.50	0.67	0.27	**−4.30**	0.80	0.37	−0.21
Ir	0.33	0.40	0.33	0.56	−0.01	−0.03	−0.42	−0.09	**−2.11**	−0.49	−0.59
Pt	0.35	0.53	0.54	0.78	0.12	0.24	0.02	0.19	0.29	**−2.25**	−0.08
Au	0.53	0.74	0.71	0.70	0.47	0.67	0.35	0.12	0.79	0.43	**−3.56**

The impurity/overlayer atoms are listed horizontally and the host entries are listed vertically. The surfaces considered are the closest packed, and the overlayer structure are pseudomorphic. All values are in eV, and the e_d values are relative to the Fermi level (reprinted with permission from [31], copyright 2007 Elsevier)

transfer to minimize the system energy. The process is usually accompanied by chemical bond breakage/formation, including chemisorption and intermediate generation. The d-band center of metals relative to the Fermi level, ε_d, has been identified as a good measure for describing the strength of interaction with reacting species [25–29]. Nørskov and coworkers have calculated ε_d values of different metals as well as their alloys and overlayer structures (Table 7.2) [30]. They have achieved promising successes in using the data for explaining chemisorption of molecules to metals.

From Table 7.2, we learn that the ε_d alters with metals, which helps to explain why they have different interaction with reacting species and exhibit different electrocatalytic property. For example, the platinum group metals (including Ru,

Rh, Pd, Ir, and Pt) are effective electrocatalyst for CO electro-oxidation reaction, whereas the coinage metals (including Cu, Ag, and Au) are inactive toward this reaction [32–34]. The little activity of coinages metals could be attributed to their significantly deeper d-band centers comparing to the platinum group metals, which leads to much weaker interaction with CO molecules. The arguments are in good consistence with Fourier transform infrared spectroscopy (FTIR) studies, which observe little CO adsorption to the coinage metals but strong CO adsorption to the platinum group metals.

Another important message drawn from Table 7.2 is that the ε_d of metals can be adjusted by alloying or creating heterogeneous overlayers. The shift in ε_d has been attributed to charge transfer and/or lattice change due to incorporation of a second metal. For instance, the ε_d of pure Pt is −2.25 eV, which enables Pt to interact moderately with many reacting species and makes it an active catalyst for a variety of electrochemical reactions, for instance oxygen reduction reaction (ORR), methanol oxidation reaction (MOR), and ammonia oxidation reaction (AOR) [20, 35–42]. Fundamental studies have suggested a more negative ε_d for Pt in ORR to suppress the adsorption of hydroxyl species, which compete with ORR and negatively influence the reaction kinetics. From Table 7.2, the ε_d for surface Pt can be shifted negatively when it is alloyed with selected elements (Pt-M, M = Fe, Co, Ni, Cu, etc) or is overlayered on these metals. In experiments, these alloys and overlayer structures have been demonstrated with improved ORR kinetics than pure Pt [43–47], which validates the d-band theory.

7.4.2 Geometric Effect

The physical structure of metals depends primarily on the arrangements of atoms that make up the metals. Most of metal electrocatalyst nanoparticles are crystalline in structure, i.e., the metal atoms being arranged in a pattern that repeat themselves in three dimensions. Body-centered cubic (*bcc*), face-centered cubic (*fcc*), and hexagonal close-packed (*hcp*) structures are most often observed for crystalline metals. The atom arrangement, or geometry, can vary significantly with different crystal structure and planes. Correspondingly, the geometric structure of metal surface can be greatly altered by exposing different crystal planes. Figure 7.6 shows the geometric structure of (100), (110), and (111) surface planes of an *fcc* structure, which have different atom arrangements and atom-atom distances.

It is often that multiple active sites are required simultaneously to catalyze electrochemical reactions. How these metal active sites arrange can thus dramatically alter their interaction with the reacting species, which lead to an altered reaction kinetics. These kind of electrochemical reactions are grouped as surface sensitive reactions, in which the surface geometry of metal nanoparticles can play a determining role. For instance, CO can be oxidized into CO_2 under Pt electrocatalysis, and the reaction is found sensitive to Pt surface. Mechanistic studies suggest an Eley–Rideal (E-R) mechanism in an alkaline solution [48]:

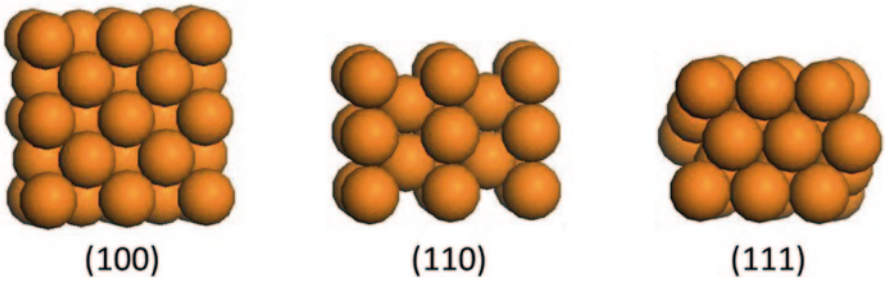

Fig. 7.6 Schematic illustration of (100), (110), and (111) surface planes of *fcc* metals

$$CO_{ads} + 2OH^- \rightarrow CO_2 + H_2O + 2e^- \tag{7.26}$$

Adsorbed CO molecules on Pt react with OH^- in the bulk phase, which leads to production of CO_2 and H_2O and meanwhile generation of electrons. Figure 7.7 shows the voltammetric CO oxidation on single crystalline Pt (111), (110), and (100) [48]. The main anodic peaks are resulted from E-R CO oxidation, while the small shoulder peaks in the double layer region are attributed to the reaction between CO_{ads} and OH_{ads} adsorbed on defect sites via a Langmuir–Hinshelwook (L-H) mechanism. The reaction exhibits varying onset potentials on different Pt surfaces, following the order $E_{Pt(110)} < E_{Pt(100)} < E_{Pt(111)}$. It suggests different reaction kinetics in order of $i_{0,Pt(110)} > i_{0,Pt(100)} > i_{0,Pt(111)}$. A plausible explanation is that CO molecules form multiple bonds with Pt active sites when they adsorb to the surface. The CO_{ads} on Pt (111) is primarily triple bonded while the CO_{ads} on Pt (110) and (100) are less bonded due to geometric constraint. The more stabilized CO_{ads} on Pt (111) cause a larger E_A and thus a smaller i_0 for electro-oxidation comparing to that on the other two Pt surfaces.

7.4.3 Other Effects

Besides the electronic and geometric structures of metals in controlling the intrinsic kinetics of electrochemical reactions, some other factors can also play an important role. Here, we briefly discuss two major effects which often involve in metal electrocatalysis.

7.4.3.1 Third-Body Effect

A third-body effect describes the role of second metal atoms, which by themselves are inactive and do not directly involve in electrocatalysis, in blocking the active sites for a side reaction or in blocking the adsorption of poisoning species, which require multiple adjacent active sites for adsorption. In this effect, the second metal

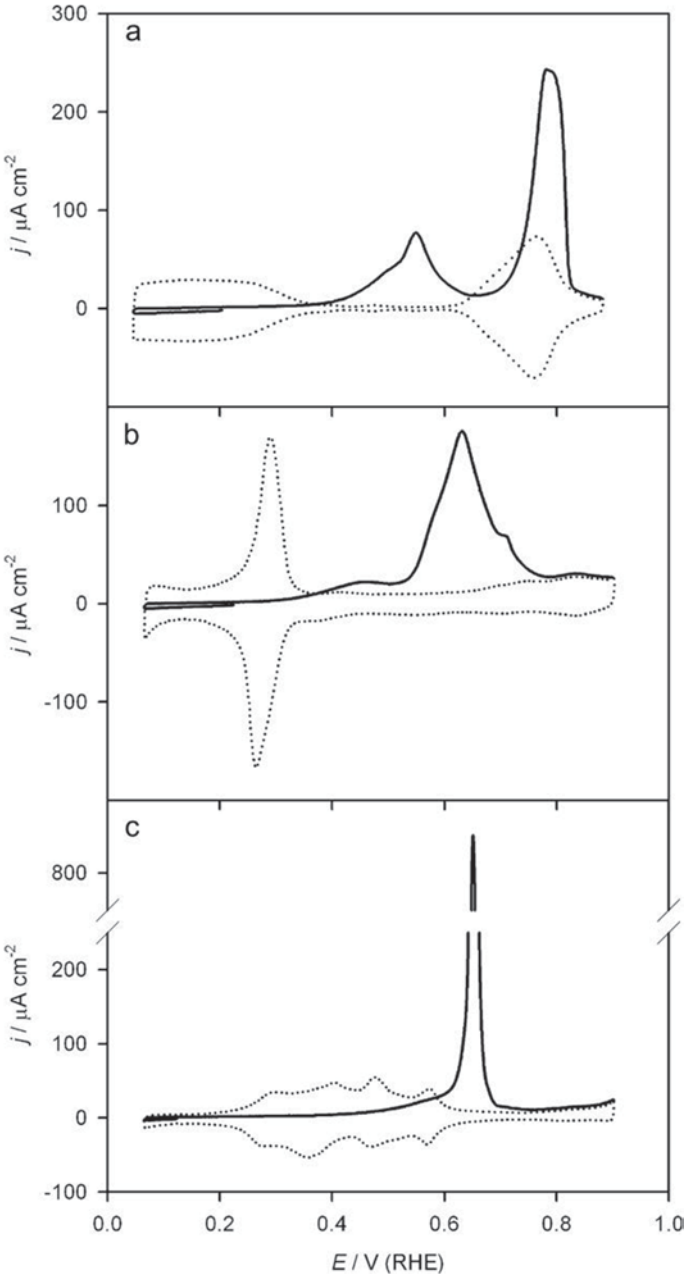

Fig. 7.7 Electrochemical oxidation of adsorbed CO on Pt (hkl) in 0.1 M NaOH solution: (a) Pt (111), (b) Pt (110), and (c) Pt (100). Scan rate = 50 mV/s, background CV (*dotted line*) collected immediately after CO stripping (reprinted with permission from [48], copyright 2004 Elsevier)

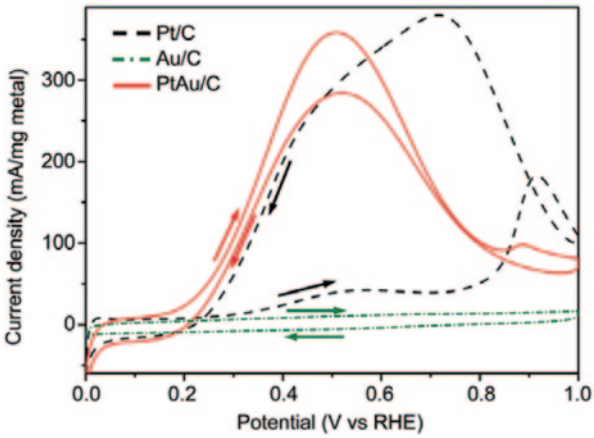

Fig. 7.8 Cyclic voltammetry curves of FAOR using Pt/C, Au/C, and PtAu/C alloy nanoparticles (reprinted with permission from [49], copyright 2009 Springer)

atoms does not improve the reaction turnover frequency (TOF) on individual active sites of the first metal, but alter the distribution of reaction pathways by breaking the active sites into smaller ensembles.

One example is the formic acid electro-oxidation reaction (FAOR), which have two major reaction pathways (dehydrogenation and dehydration) under metal electrocatalysis [49]:

$$HCOOH \xrightarrow{dehydrogenation} CO_2 + 2H^+ + 2e^- \tag{7.27}$$

$$HCOOH \xrightarrow{dehydration} CO_{ads} + H_2O \rightarrow CO_2 + 2H^+ + 2e^- \tag{7.28}$$

FA molecules are directly electro-oxidized to CO_2 in a dehydrogenation pathway, while CO_{ads}-like intermediates are first generated and then oxidized to CO_2 in a dehydration pathway. The reaction occurs via both pathways when pure Pt is used. The generated CO_{ads} through FA dehydration readily adsorb to Pt and block the active sites for further FAOR, causing decreased amount of the active sites and thus diminished activity (Fig. 7.8) [49]. PtAu alloy nanoparticles exhibit significantly higher activity than pure Pt, which can be attributed to the third-body effect. Although Au is inert for FAOR, it can modify the Pt surface by breaking the Pt atoms into smaller ensembles. As the dehydration path requires multiple adjacent Pt sites, it is effectively suppressed due to decreased availability of such site ensembles. The FAOR thus primarily undergoes the dehydrogenation pathway on PtAu and generates less CO_{ads} poisoning species than on pure Pt, leading to increased reaction rate and thus current density.

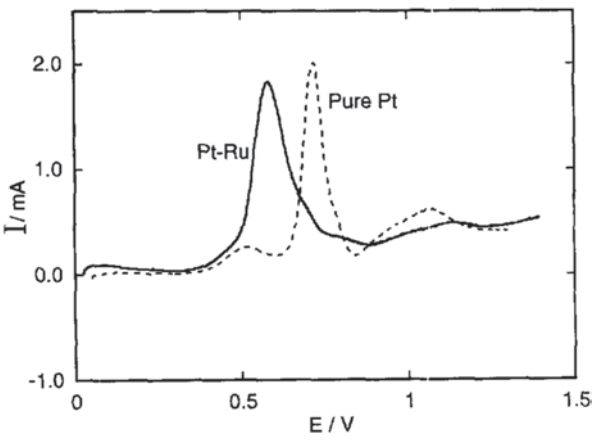

Fig. 7.9 Electrochemical oxidation of adsorbed CO on pure Pt and bimetallic Pt–Ru electrodes in 3 M H_2SO_4 at 10 mV/s (reprinted with permission from [50], copyright 1998 Elsevier)

7.4.3.2 Bifunctional Effect

In the bifunctional effect two types of active sites, which have distinct roles in the electrochemical reaction, are in presence and in close adjacency. It is often that an electrochemical step involves two reacting species, both of which need activation but impose different requirements on the active sites. A good catalyst needs to contain two types of active sites, which function together to activate both species and to ensure efficient reaction between the two species.

For example, electro-oxidation of adsorbed CO on Pt ($CO_{ads,\ Pt}$) in an acid electrolyte is considered following a L-H mechanism [50]:

$$H_2O + Pt \rightarrow OH_{ads,Pt} + H^+ + e^- \tag{7.29}$$

$$CO_{ads,Pt} + OH_{ads,Pt} \rightarrow CO_2 + H^+ + e^- \tag{7.30}$$

The reaction has little activity below 0.6 V vs. reversible hydrogen electrode (RHE), which is limited by Step (7.29) because pure Pt cannot effectively adsorb OH species until the potential (Fig. 7.9). Bimetallic Pt–Ru is discovered to be a better electrocatalyst for this reaction, with more negative onset potential (i.e., bigger i_0) comparing to pure Pt. One plausible explanation is that Ru adsorbs OH groups efficiently at low potentials, which react with adsorbed CO on Pt sites:

$$H_2O + Ru \rightarrow OH_{ads,Ru} + H^+ + e^- \tag{7.31}$$

$$CO_{ads,Pt} + OH_{ads,Ru} \rightarrow CO_2 + H^+ + e^- \tag{7.32}$$

The reaction mechanism is altered by using the bimetallic Pt–Ru, in which Ru promotes the OH adsorption and Pt promotes the CO adsorption. They function together to catalyze the reaction at a lower potential than pure Pt.

It needs to be noted that all the four effects are functions of the physical parameters of metal electrocatalyst, some of which are common. Adjustment in one physical parameter can lead to variations in multiple effects. In another word, it is often that multiple effects work simultaneously to determine the electrochemical reaction kinetics, although one of them might play a dominating role. For instance, the higher FAOR activity on PtAu alloy than on pure Pt can be mainly attributed to a third-body effect (Chap. 7.4.3.1), in which surface Au atoms by themselves are inert for the reaction. Their presence helps to break surface Pt atoms into discontinuous ensembles, suppresses the undesired pathway, and leads to increased reaction rate. Besides the third-body effect, the addition of Au atoms also alters the geometric structure of the particle surface. It is because that Au and Pt have different atom size and electron affinity, which cause surface restructuring and changes in the lattice parameters. From Table 7.2, the ε_d for surface Pt shifts up when being alloyed with Au, which indicates an alteration of the electronic structure. Thus, besides the dominating third-body effect, the geometric and electronic effects could also possibly play a role in the FAOR reaction. Because of the fact that multiple effects can work together and influence each other, it is sometimes difficult to disentangle their separate impact on the reaction. A synergistic effect, a more general term which describes the creation of an effect greater than the sum of individual effects due to the interaction of multiple elements in electrocatalyst, is sometimes used to include all possible effects.

7.4.4 Practical Considerations in Metal Electrocatalyst Research

Some practical issues also need consideration in the metal electrocatalyst research. It is because metals have their own physical and chemical properties, which can affect and even determine the electrochemical property.

7.4.4.1 Chemical Stability of Metals

The chemical stability of metals requires practical consideration in researching metal electrocatalyst. A good metal electrocatalyst should well maintain its structure and chemical identity under the working condition. For instance, mechanistic studies suggest a down-shift in the d-band center of Pt, which has a ε_d of -2.25 eV, for promoting the ORR kinetics [51]. If we only consider the electronic effect, Cu has a moderately deeper ε_d of -2.67 eV and could be expected to be a better electrocatalyst than Pt. However, Cu is not a suitable ORR catalyst at all. It has a low redox potential and can readily dissolve in acid electrolyte in the ORR potential range. Moreover, the low redox potential of Cu causes high coverage of OH species even at low potentials, which compete with ORR and negatively influence the

Table 7.3 Standard redox potentials for metals

Half-cell reaction	$E^0_{C/A}$ (V vs. SHE)
$Fe^{2+} + 2e^- \Leftrightarrow Fe$	−0.447
$Co^{2+} + 2e^- \Leftrightarrow Co$	−0.28
$Ni^{2+} + 2e^- \Leftrightarrow Ni$	−0.257
$Cu^{2+} + 2e^- \Leftrightarrow Cu$	0.342
$Ru^{2+} + 2e^- \Leftrightarrow Ru$	0.455
$Rh^{3+} + 3e^- \Leftrightarrow Rh$	0.758
$Pd^{2+} + 2e^- \Leftrightarrow Pd$	0.951
$Ag^{+} + e^- \Leftrightarrow Ag$	0.7996
$Ir^{3+} + 3e^- \Leftrightarrow Ir$	1.156
$Pt^{2+} + 2e^- \Leftrightarrow Pt$	1.18
$Au^{3+} + 3e^- \Leftrightarrow Au$	1.498

reaction kinetics. Another example is the intermetallic PtPb electrocatalyst for both MOR and FAOR at low potential range [52, 53]. It is discovered as significantly better catalyst for the two reactions than pure Pt, which could possibly be attributed to a combination of third-body and bifunctional effects. The Pb surface atoms can effectively adsorb OH groups at low potentials, which serve as one of the reacting species, and break surface Pt atoms into smaller ensembles, which help to suppress the undesired pathway. They function synergistically with Pt active sites for promoting the reaction kinetics. However, it is observed the intermetallic PtPb rapidly loses the activity if the working electrode is ramped to potentials above the Pb redox potential. It is because Pb begins to leach out above the potential, which leaves a pure Pt surface and loses the third-body and bifunctional effects. Table 7.3 lists the equilibrium redox potential for some metals under the standard condition ($E^0_{A_{x+}/A}$), which can be used as a qualitative measure for evaluating their chemical stability under the working condition.

7.4.4.2 Metal Surface Restructuring and Segregation

Another practical consideration in the electrocatalyst research is restructuring and/or segregation of metal surfaces, which affect the catalytic property by altering the surface geometry. The real surface of working metal electrocatalyst, which is often resultant of complex interplays between many factors, including surface restructuring, surface segregation, and surface interaction with reacting species, can be quite different from the ideal bulk structure.

It is a general phenomenon that the surface atoms can restructure and have different arrangement from those in the bulk, which is driven by a positive surface energy. The surface atoms can also restructure under the interaction with reacting

species. For instance, *fcc* Pt (100) surface under vacuum consists of a quasi-hexagonal structure, rather than the square symmetry (100) lattice. The surface restructuring is driven by the surface energy minimization. When the Pt (100) is exposed to CO atmosphere, CO molecules adsorb to the surface and can cause restructuring of the quasi-hexagonally arranged surface Pt atoms back into a square-like structure. This surface restructuring process is driven by the interaction between adsorbed CO and surface Pt atoms [54].

Surface aggregation often occurs in alloys, which causes a different surface composition from the bulk phase. The phenomenon is originated from the different property between elements, including metal–metal bond strength and atom size. Norskov and coworkers have calculated the segregation energies of all binary combinations of transition metals (Fig. 7.10) [28], which provide a valuable measure to estimate the tendency of metals to segregate in their alloy surfaces. For instance, Pt–Ru is among the most active electrocatalysts for MOR [55–59]. From the calculated segregation energies, we learn that Ru strongly antisegregates when being alloyed with Pt, whereas Pt strongly segregates when being alloyed with Ru. The resultant surface structure under such segregation effects consists of separate Ru sites, each of which is surrounded by several Pt atoms. Such a surface structure is favorable for MOR, with the isolated Ru sites to provide OH species and the adjacent Pt sites to activate methanol oxidation.

7.5 Current Development of Metallic Nanostructures for Electrocatalysis

As the electrochemical reactions differ from each other in many aspects, including reaction mechanism, intrinsic kinetics, reaction conditions, and so on, the imposed requirements on metal electrocatalyst are often different. As a result, different electrochemical reactions are found with different metallic nanostructures as the best performed catalyst. In general, a good metal electrocatalyst for an electrochemical reaction possesses the following characteristics: (1) it exhibits excellent activity toward the reaction; (2) it is chemically stable and durable under the reaction condition; and (3) it is cost-effective. Here we briefly introduce a few important electrochemical reactions and discuss the current catalyst development.

7.5.1 Oxygen Electrochemistry

7.5.1.1 Oxygen Reduction Reaction

Oxygen reduction reaction (ORR) has been intensively studied over the past few decades because of its fundamental complexity and practical importance for many applications, including PEMFCs and metal–air batteries. The overall reaction in an acidic electrolyte can be described as follows:

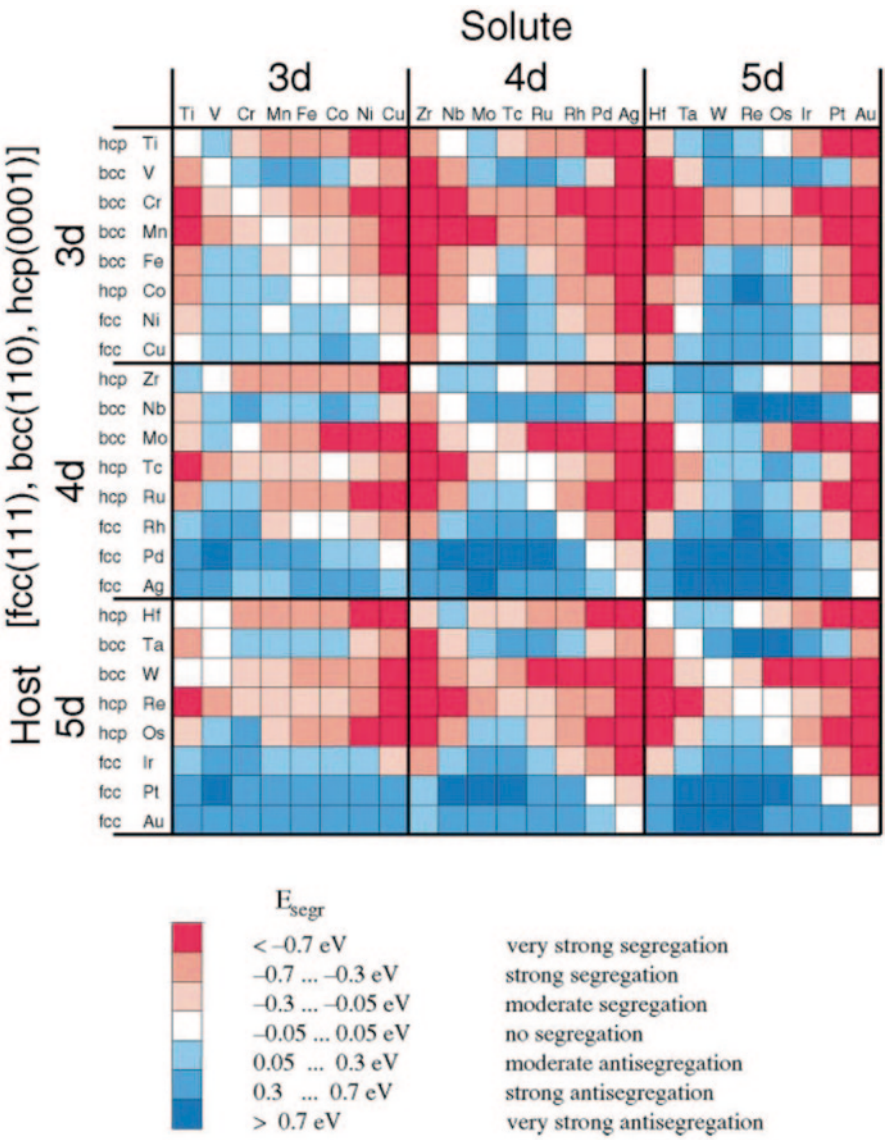

Fig. 7.10 Surface segregation energies for transition metal solutes in the close-packed surfaces of transition metal hosts (reprinted with permission from [28], copyright 2002 Annual Reviews)

$$O_2 + 4H^+ + 4e^- \rightarrow 2H_2O \quad (E_0 = 1.229\,\text{V vs. SHE}) \tag{7.33}$$

There are two difficulties in the research of ORR metal electrocatalysts. One is the low intrinsic exchange current density, i_0, which leads to very sluggish reaction kinetics and large overpotential. The other is the high working potential in acidic electrolyte, which imposes rigid requirement on the chemical stability of metals.

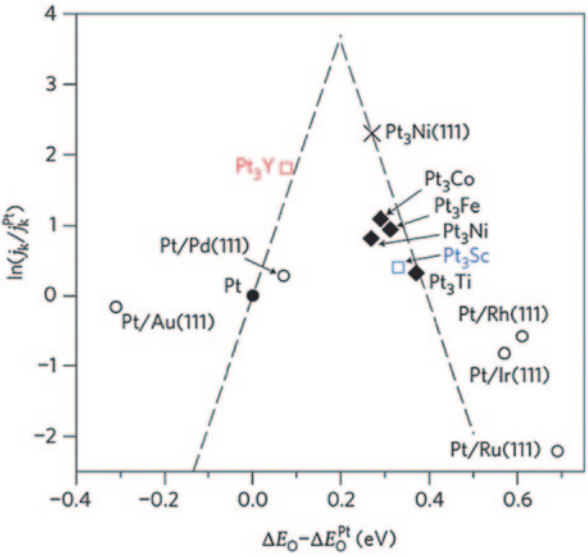

Fig. 7.11 Experimental kinetic current density of metal electrocatalysts as a function of the calculated oxygen adsoprtion energy, ΔE_O, with respect to that of Pt (111) (reprinted with permission from [51], copyright 2013 Royal Society of Chemistry)

Pt has been found the most effective metal for both reaction kinetics and stability considerations. However, even the i_0 can be increased to around 10^{-10} A/cm^2 using Pt, it is still not sufficient for the reaction [60]. The current state-of-the-art Pt/C catalyst exhibits around 0.2 mA/cm^2 Pt and 0.2 A/mg Pt at 0.9 V vs. RHE in ORR [20]. Large amount of expensive Pt metal is needed to generate usable currents with high energy conversion efficiency in both PEMFCs and metal–air batteries. To advance these technologies the Pt usage must be dramatically reduced, with targets of 0.7 mA/cm^2 Pt and 0.44 A/mg Pt at 0.9 V vs. RHE being set by the DOE [61]. Intensive research activities have been conducted in search of active Pt structure in the past years to reach the targets, which led to the development of many types of alloy [62–68], skin-layer [69–72], core-shell and thin-film electrocatalysts [73–76].

Mechanistic studies on Pt suggest that the ORR begins with adsorption of O_2 to the active sites (Eq. 7.34), which is a fast process. The adsorbed O_2, $O_2 \cdot S$, gains one electron from the electrode and reacts with one proton to generate active intermediate HOO·S (Eq. 7.35), which is further electroreduced to H_2O.

$$O_2 + S \Leftrightarrow O_2 \cdot S \quad \text{(fast)} \tag{7.34}$$

$$O_2 \cdot S + H^+ + e^- \Leftrightarrow HOO \cdot S \quad \text{(rate-limiting step)} \tag{7.35}$$

The HOO·S generation is discovered to be the rate-limiting step on Pt [77], which determines the i_0 value and controls the ORR kinetics. The oxygen adsorption energy to the metal surface (ΔE_O), which is a function of the metal electronic structure, has been found an effective descriptor for the reaction. A valcano-like relationship between the ORR activity and ΔE_O has been discovered (Fig. 7.11), suggesting an optimal ΔE_O for a perfect metal electrocatalyst [51].

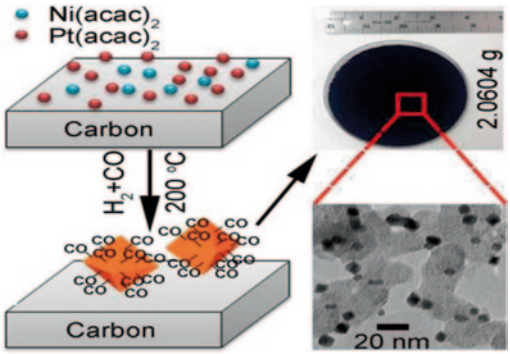

Fig. 7.12 Preparation and TEM of octahedral Pt–Ni nanoparticles on C support using solid-state chemistry (reprinted with permission from [61], copyright 2014 American Chemical Society)

Studies show that single crystalline Pt_3Ni (111) can be about 90 times more active than the state-of-the-art Pt/C [62]. The largely improved kinetics could be attributed to a down-shift in the ε_d of surface Pt and the (111) surface geometry. A plausible explanation is that the rate-limiting step favors a more negative ε_d (or a less negative ΔE_O) comparing to that of pure Pt. Meanwhile, the (111) surface geometry is also favored to decrease the surface coverage of adsorbed OH species, which negatively influence the reaction by blocking the active sites for Eq. 7.35. The discovery has motivated the research of octahedral Pt–Ni alloy nanoparticles, which are enclosed by the (111) planes and have large specific active area [62, 63, 78–81].

Peng and coworkers has recently developed a scalable, surfactant-free, and low-cost solid-state chemistry method for making octahedral Pt–Ni alloy nanoparticles on carbon support (Pt-Ni/C) [61]. In the method, octahedral Pt–Ni/C can be prepared by simply impregnating both platinum and nickel acetylacetonates onto C support and reducing them at 200 °C in 120/5 cm^3/min CO/H_2 for 1 h. Mechanistic studies suggest that the octahedral Pt–Ni production is resultant of employing both CO and H_2 gases, wherein H_2 aids transportation and reduction of the metal precursors on C support and CO is responsible for the particle morphology formation. Figure 7.12 shows the schematic illustration of the method and the produced octahedral Pt–Ni nanoparticles.

The octahedral Pt–Ni/C nanoparticles with different composition were studied for the ORR property, which exhibit significantly higher activity than the commercial Pt/C (Fig. 7.13). The octahedral $Pt_{1.5}Ni$/C shows the highest activity, with a j_{area} of 3.99 mA/cm^2 Pt being harvested at 0.90 V vs. RHE. It is about 20 times of the value for the Pt/C (0.2 mA/cm^2 Pt). The j_{mass} of the octahedral $Pt_{1.5}Ni$/C is 1.96 A/mg Pt and is 10 times as high comparing to the Pt/C (0.19 A/mg Pt). However, the long-term stability of the octahedral Pt-Ni/C catalyst remains a challenge. After 4000 cycles of linear potential sweeps between 0.60 and 1.00 V vs. RHE at a scan rate of 50 mV/s, the j_{area} and j_{mass} for the $Pt_{1.5}Ni$/C decrease to 2.17 mA/cm^2 Pt and 0.97 A/mg Pt at 0.9 V vs. RHE, although the electrochemical active surface area (ECSA) decays by only 8 %. The instability of the octahedral Pt–Ni/C could be attributed to a gradual Ni dissolution, which is chemically unstable in acid and under high potential and tends to leach out.

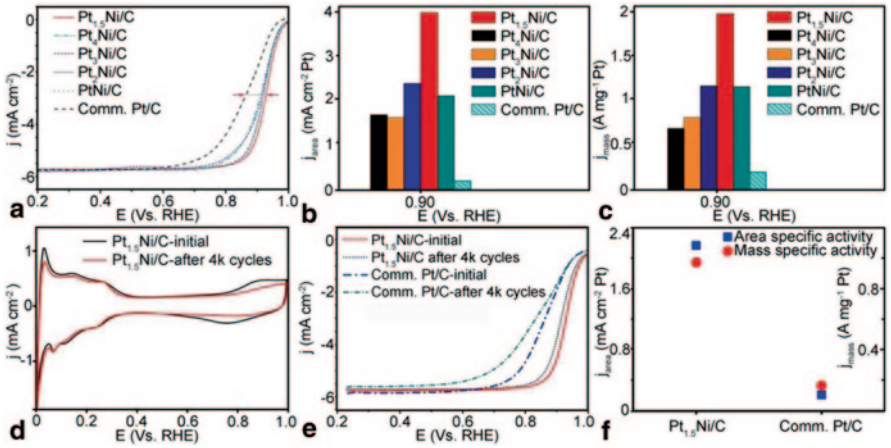

Fig. 7.13 ORR property of octahedral Pt–Ni/C. **a** ORR polarization curves and **b**, **c** active area and mass-specified ORR current densities (j_{area} and j_{mass}) of PtNi/C, $Pt_{1.5}Ni/C$, Pt_2Ni/C, Pt_3Ni/C, Pt_4Ni/C, and commercial Pt/C in O_2-saturated 0.1 M $HClO_4$ at room temperature, with a scan rate of 10 mV/s and an electrode rotating rate of 1600 rpm, and **d** Cyclic voltammograms, **e** ORR, and **f** j_{area} and j_{mass} of $Pt_{1.5}Ni/C$ and commercial Pt/C after accelerated stability test (reprinted with permission from [61], copyright 2014 American Chemical Society)

7.5.1.2 Oxygen Evolution Reaction

Oxygen evolution reaction (OER) differs from ORR in the reaction mechanism, although it is considered as the reverse process of ORR. Thus, the characteristics of a good OER catalyst are different from that for ORR. The OER catalyst research is of particular interest for water splitting, and regenerative fuels cells and batteries. Mechanistic studies suggest the following OER pathway on metals in acidic electrolyte [60, 82]:

$$H_2O + S \Leftrightarrow HO \cdot S + H^+ + e^- \tag{7.36}$$

$$HO \cdot S \Leftrightarrow O \cdot S + H^+ + e^- \tag{7.37}$$

$$O \cdot S + H_2O \Leftrightarrow HOO \cdot S + H^+ + e^- \tag{7.38}$$

$$HOO \cdot S \Leftrightarrow S + O_2 + H^+ + e^- \tag{7.39}$$

It is proposed that Eq. 7.37 is the rate-limiting step when the active sites interacts weakly with oxygenated species, while Eq. 7.38 is the rate-limiting step if the interaction is strong. Based on the mechanism, metals are actually more in their oxidative state during electrocatalysis.

A perfect OER catalyst must have optimal interaction with oxygenated species to balance the kinetics between the two steps. A valcano plot has been obtained

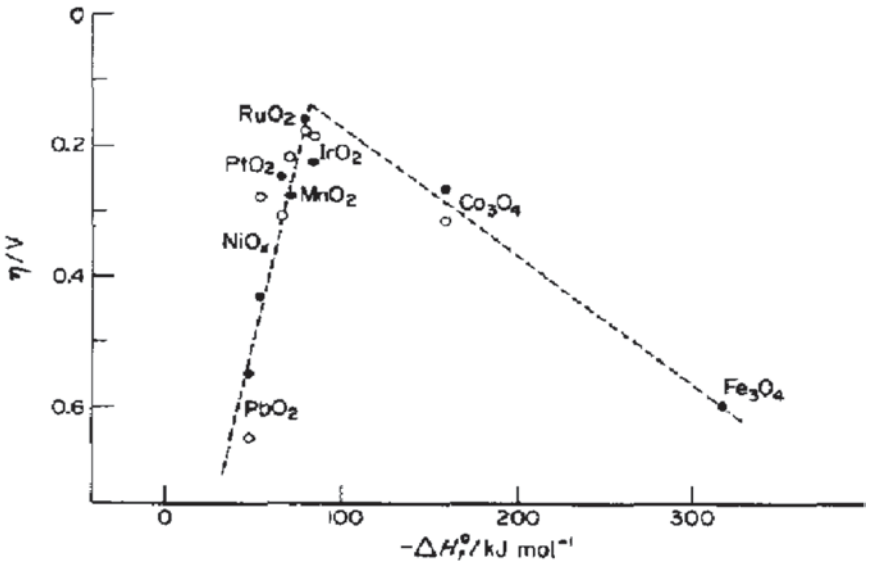

Fig. 7.14 Volcano plot of the overpotential for OER vs. the enthalpy of the lower to higher oxide transition. *Solid circles*: in acidic electrolyte, *hollow circles*: in alkaline electrolyte (reprinted with permission from [82], copyright 1984 Elsevier)

for the OER performance using different metals (Fig. 7.14) [82]. The change of enthalpy for metal oxidation has been found a good descriptor for predicting the OER property. Ru and Ir possess the most moderate values among all metals and are thus found the most effective elements for the reaction. In practice, Ru and Ir oxide nanoparticles are often used as OER electrocatalyst.

7.5.2 Hydrogen Electrochemistry

7.5.2.1 Hydrogen Evolution Reaction

Hydrogen evolution reaction (HER) receives considerable attention in recent years for H_2 production via electrochemical and photo-electrochemical water splitting. The reaction in an acidic electrolyte can be written as follows [51]:

$$2H^+ + 2e^- \rightarrow H_2 \quad (E_0 = 0.00\text{V vs. SHE}) \tag{7.40}$$

The reaction pathway on metals is proposed as follows:

$$H^+ + e^- + S \Leftrightarrow H{\cdot}S \quad \text{(rate-limiting step)} \tag{7.41}$$

$$H{\cdot}S + H{\cdot}S \Leftrightarrow H_2 + 2S \tag{7.42}$$

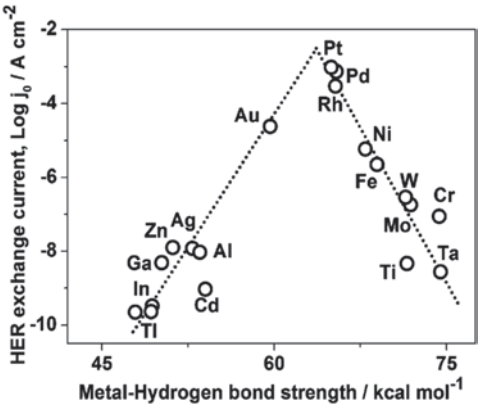

Fig. 7.15 The HER activity on metals as a function of the metal–hydrogen bond strength (reprinted with permission from [51], copyright 2013 Royal Society of Chemistry)

A valcano-like relationship for the HER kinetics has been discovered as function of the metal–hydrogen bond strength, which can be related to the electronic structure of metal surfaces (Fig. 7.15) [51]. Pt possesses the most optimal metal–hydrogen interaction among all the metals and thus exhibits the highest HER activity. Pt/C nanoparticles are often used as HER electrocatalyst.

7.5.2.2 Hydrogen Oxidation Reaction (HOR)

Hydrogen oxidation reaction (HOR) is the reverse process of HER and serves as the anode half-cell reaction for PEMFCs. Similar to HER, Pt is the most effective metal in HOR for its optimal electronic interaction with hydrogen, and is thus most often used as the electrocatalyst. It needs noted that the i_0 value for HOR on Pt can reach 10^{-3} A/cm^2 [83], which is around several orders of that for ORR on Pt. Much less amount of Pt is needed for HOR than for ORR. Thus, the electrocatalyst development is more focused on ORR side in the PEMFC research.

7.5.3 Electrochemistry of Carbon-Containing Compounds

7.5.3.1 Methanol Oxidation Reaction

Methanol has been considered as an alternative fuel for constructing direct methanol fuel cells (DMFCs), in which methanol oxidation reaction (MOR) serves as an anode reaction. The reaction has slow kinetics because of its complex reaction pathway. Despite the many mechanistic studies, the clear MOR mechanism is still under active debates. Figure 7.16 shows a multipathway scheme for the reaction, which is proposed based on the intermediate species identified in experiments [84]. Several routes involve the generation of CO_{ads}-like species, which can accumulate on metal surface and block the active sites. Pure Pt exhibits a low activity toward MOR, which is probably caused by a poisoning effect by the generation of CO_{ads}.

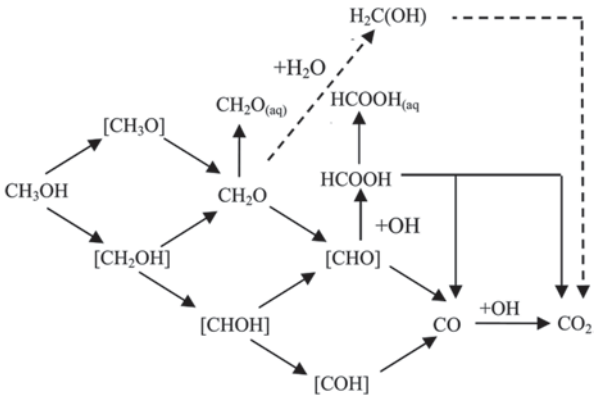

Fig. 7.16 Multipathway scheme for MOR on metal surface, with pathway in *dashed line* not being well documented (reprinted with permission from [84], copyright 2008 Springer).

Based on current understanding of the reaction, a good MOR electrocatalyst should effectively suppress CO_{ads} generation and efficiently remove generated CO_{ads}. PtRu/C alloy nanoparticles have been found a better catalyst than pure Pt for the reaction. The property improvement has been attributed to both the third-body and bifunctional effects. As being discussed in Chap. 7.4.3, the incorporation of Ru breaks surface Pt atoms into smaller ensembles, which helps to suppress CO_{ads} generation because the process requires multiple adjacent Pt sites. Meanwhile, surface Ru atoms adsorb hydroxyl species (OH_{ads}), which helps to react with and thus remove CO_{ads}. Abruna and coworkers have recently prepared PtPb intermetallic nanoparticles, which exhibit exceptionally higher MOR activity [52]. They reported one to two orders of increase in the current density and no detectable CO_{ads} formation comparing to pure Pt. They concluded that the CO_{ads} generation pathway was completely suppressed for MOR on the intermetallic PtPb (Fig. 7.17).

7.5.3.2 Formic Acid Oxidation Reaction

As being discussed in Chap. 7.4.3, formic acid oxidation reaction (FAOR) have major dehydrogenation and dehydration pathways in parallel (Eqs. 7.27 and 7.28) [49]. The dehydration pathway generates CO_{ads}, which can poison metal electrocatalyst by blocking the active sites. Pure Pt is a poor catalyst for the reaction, with the low activity caused by CO_{ads} accumulation on the surface. Pure Pd exhibits significantly higher FAOR activity than Pt [85–89]. Spectroscopic studies suggest that FAOR favors the dehydrogenation pathway on Pd comparing to Pt, which could be attributed to the electronic effect. The dehydration pathway and thus CO_{ads} generation are suppressed on Pd, leading to improved FAOR rate.

The FAOR kinetics can also be improved by adding a second metal for modifying the Pt surface. A range of PtM (M=Au, Bi, Pb, etc) alloy nanoparticles exhibit greatly improved FAOR kinetics comparing to pure Pt [90–97]. Similar to the alloy electrocatalysts for MOR, the improvement can be attributed to the third-body and/or bifunctional effect. Peng et al. has recently demonstrated the importance of Pt

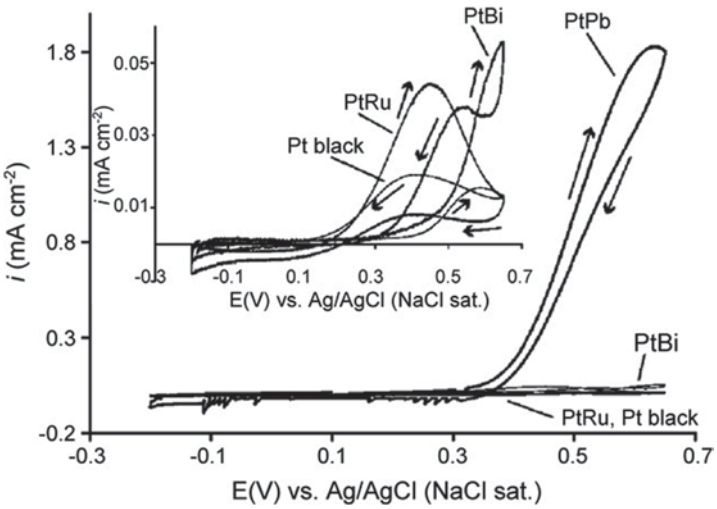

Fig. 7.17 Cyclic voltammogram for MOR using carbon-supported Pt and PtM (M = Bi, Pb, and Ru) alloy nanoparticles (reprinted with permission from [52], copyright 2006 American Chemical Society)

surface composition in affecting the FAOR by studying PtAg alloy electrocatalyst (Fig. 7.18) [98]. In the study $Pt_{18}Ag_{82}$ alloy nanoparticles were first synthesized by reducing Pt acetylacetonate and Ag stearate in a mixture of 1,2-hexadecanediol, oleylamine, oleic acid, and dipenyl ether at 200 °C, and then put on a C support for preparing $Pt_{18}Ag_{82}$/C. By adjusting the potential range used for electrochemical dissolution of Ag from the $Pt_{18}Ag_{82}$, the surface composition of the particles can be well controlled. The optimal surface composition was discovered to be Pt_3Ag, which leads to an overall particle composition of $Pt_{34}Ag_{66}$, for the FAOR, with the activity being more than one order higher than that using pure Pt. In comparison, the Pt–Ag structure with a pure Pt surface, which was produced using the $Pt_{18}Ag_{82}$ by altering the electrochemical treatment potential, exhibits much less activity comparing to $Pt_{34}Ag_{66}$.

7.5.3.3 Ethanol Oxidation Reaction

Ethanol oxidation reaction (EOR) is an even more complex electrochemical reaction comparing to MOR. A complete EOR process involves C–C bond breakage, transfer of 12 electrons, and generation of many intermediate species. Figure 7.19 shows some suggested reaction routes for EOR from mechanistic studies [84]. In situ FTIR and on-line DEMS studies show that ethanol cannot be effectively electro-oxidized into CO_2 on Pt. The CO_2 yield is only about a few percent, with the major products being acetaldehyde and acetic acid. The low yield of CO_2 is caused by inefficient breakage of the C–C bond, which creates a big energy barrier and requires high energy input.

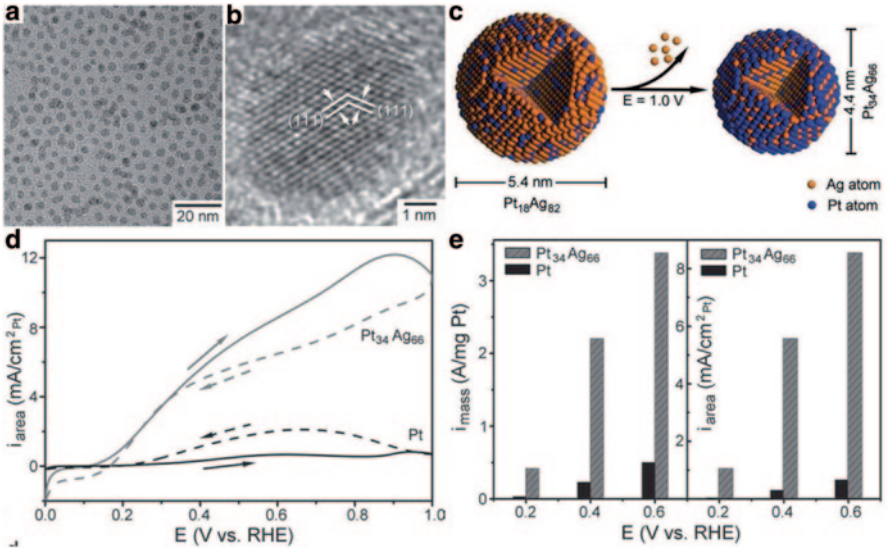

Fig. 7.18 **a** TEM and **b** HRTEM of as-synthesized $Pt_{18}Ag_{82}$ alloy nanoparticles, **c** preparation of Pt surface-rich $Pt_{34}Ag_{66}$ nanostructure by controlled electrochemical Ag dissolution from $Pt_{18}Ag_{82}$, and **d**, **e** cyclic voltammetry and FAOR activity using the Pt surface-rich $Pt_{34}Ag_{66}$ and pure Pt electrocatalysts (adapted with permission from [98], copyright 2010 Wiley-VCH)

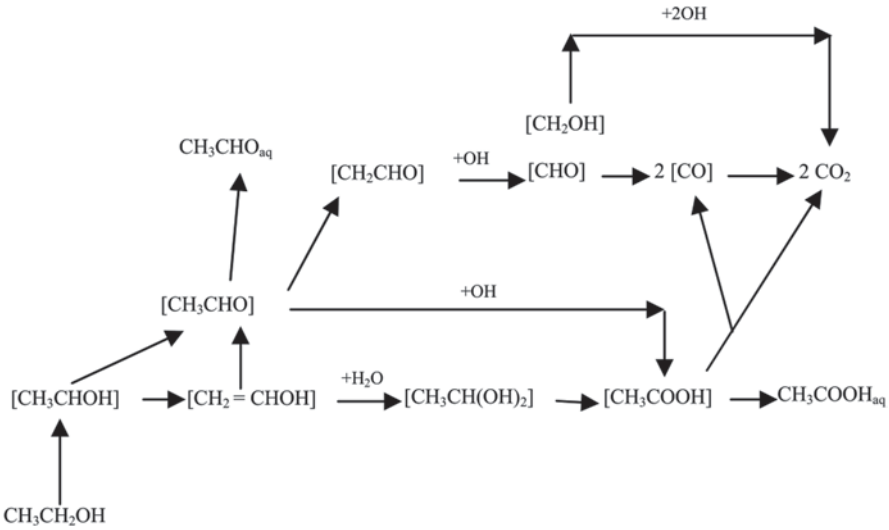

Fig. 7.19 Multipathway scheme for EOR on metal surface (reprinted with permission from [84], copyright 2008 Springer)

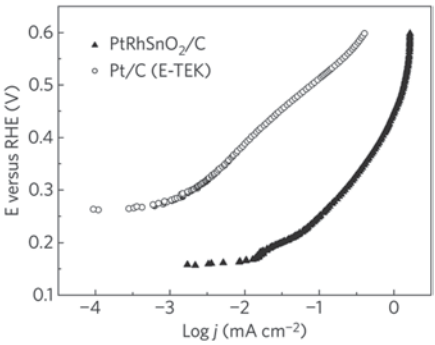

Fig. 7.20 EOR polarization curves on $PtRhSnO_2/C$ and Pt/C (reprinted with permission from [99], copyright 2009 Nature Publishing Group)

Adzic and his coworkers have recently researched a ternary $PtRhSnO_2/C$ electrocatalyst and claimed high effectiveness of the catalyst in splitting the C–C bond [99]. They prepared the $PtRhSnO_2/C$ nanoparticles using a controllable deposition called the cation-adsorption-reduction-galvanic-displacement method. The EOR activity for the $PtRhSnO_2/C$ is more than two orders of magnitude higher than that of the commercial Pt/C at 0.3 V vs. RHE. The dramatically improved activity was attributed to a synergistic effect, in which Pt facilitates ethanol dehydrogenation and modifies the electronic structure of Rh, Rh facilitates C–C bond breaking and ethanol oxidation, and SnO_2 provides adsorbed OH species to oxidize the dissociated CO at Rh sites (Fig. 7.20).

7.5.4 Electrochemistry of Nitrogen-Containing Compounds

7.5.4.1 Ammonia Oxidation Reaction

Ammonia oxidation reaction (AOR) electrocatalyzed by metals has attracted considerable interest for many potential applications, including direct ammonia fuel cells [100–102], electrochemical detection of ammonia [103], and wastewater treatment [104, 105]. Mechanistic study discovers that AOR on Pt occurs via stepwise dehydrogenation and generation of $NH_{x,ad}$ (x = 1, 2) species (Fig. 7.21) [106, 107]. The $NH_{x,ad}$ undergoes dimerization to produce $N_2H_{y,ad}$ (y = 2, 3, 4), which is the rate-limiting step. Further dehydrogenation of $N_2H_{y,ad}$ produces final product, N_2 [108–110]. Meanwhile, N_{ad} can be generated via complete dehydrogenation of $NH_{x,ad}$. The produced N_{ad} block the active sites due to strong chemisorption to Pt and largely suppress AOR activity [109]. Studies on Pt single crystals find that the reaction is geometric structure sensitive. Pt (100) is much more active than Pt (111) and (110) [111–113]. Both experimental and theoretical results also suggest less generation and easier removal of N_{ad} on Pt (100) than on other surfaces [112, 114–117]. The synergistic effect leads to a dramatically higher AOR activity.

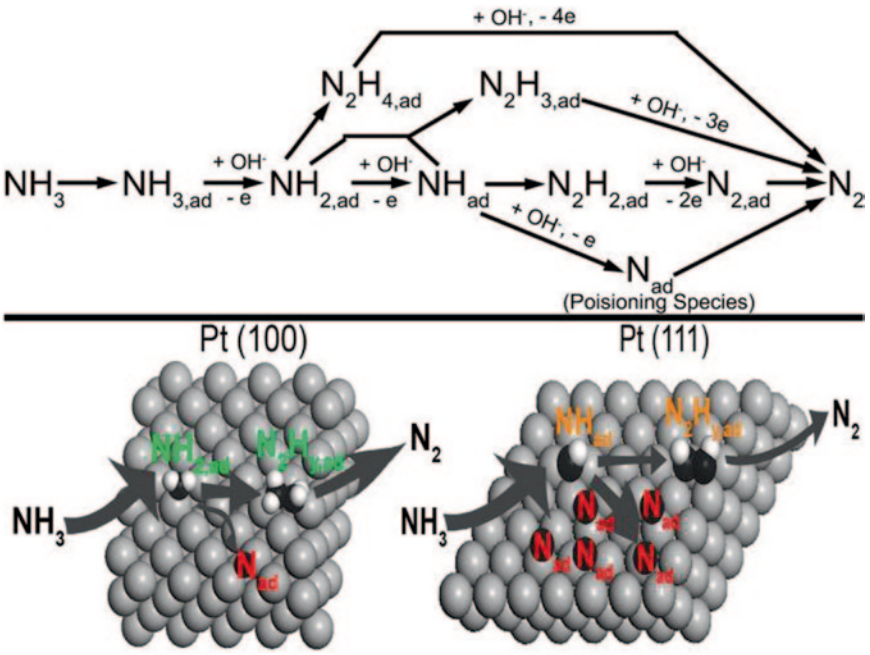

Fig. 7.21 Schematic illustration of AOR pathways on Pt (100) and (111) surfaces (reprinted with permission from [35], copyright 2013 Royal Society of Chemistry)

The finding suggests that cubic Pt nanoparticles, which are enclosed exclusively by the Pt (100) surfaces, are good AOR electrocatalyst. Peng and coworkers have recently produced cubic Pt nanoparticles on C support (PtNCs/C) using a similar solid-state chemistry method as for preparing octahedral Pt–Ni/C [35]. The PtNCs/C exhibits an AOR current density of 1.44 mA/cm^2 Pt at 0.6 V vs. RHE, which is about five times of that using the commercial Pt/C (0.30 mA/cm^2) at the same potential. The significant enhancement in the current density represents much improved reaction kinetics and demonstrates the geometric effect of Pt nanoparticles on the AOR property (Fig. 7.22).

7.5.4.2 Hydrazine Oxidation Reaction

Hydrazine oxidation reaction (HZOR) has been applied in many industrial applications, including metal plating, corrosion protection, and direct hydrazine fuel cells. It has been proposed that HZOR on metal surfaces proceeds through direct hydrazine electrochemical dehydrogenation into N_2. The reaction involves no N–N bond breakage and less electron transfer, and is thus intrinsically more active comparing to AOR. The reaction pathway in an acidic electrolyte can be depicted as follows [118]:

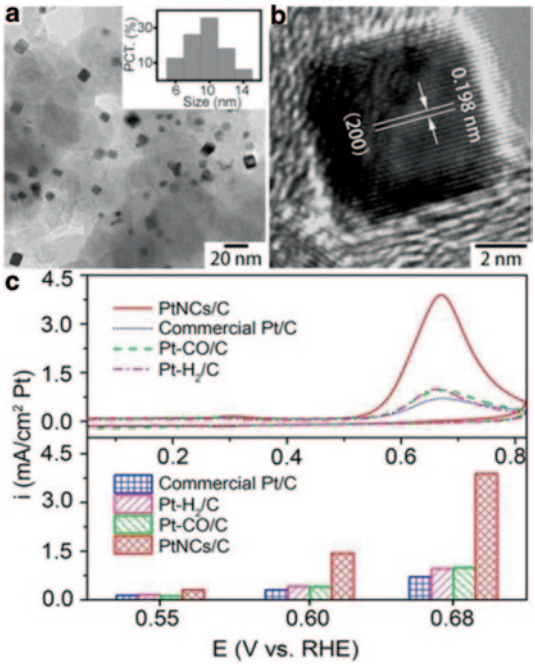

Fig. 7.22 **a** TEM and **b** HRTEM of cubic Pt/C nanoparticles (PtNCs/C) prepared using solid-state chemistry method, and **c** the AOR activity using the PtNCs/C and the commercial Pt/C (reprinted with permission from [35], copyright 2013 Royal Society of Chemistry)

$$N_2H_5^+ + S \Leftrightarrow N_2H_3 \cdot S + 2H^+ + e^- \tag{7.43}$$

$$N_2H_3 \cdot S + S \Leftrightarrow N_2H_2 \cdot 2S + H^+ + e^- \quad \text{(rate-determining step)} \tag{7.44}$$

$$N_2H_2 \cdot 2S \Leftrightarrow N_2 + 2H^+ + 2e^- \tag{7.45}$$

Step (7.44) seems to be the rate-determining step and is discovered to be both electronic and geometric structure sensitive. Dissimilar to AOR, for which Pt is the most active among all metals, Rh exhibits the highest activity for AZOR. It indicates Rh has the most optimal electronic structure for promoting the rate-limiting process. The AZOR activity on different Rh surfaces follows the trend of Rh (100) > Rh (111) > Rh (110) (Fig. 7.23). The geometric structure-dependent activity could be attributed to the active sites requirement for $N_2H_2 \cdot 2S$ species generation, in which two adjacent active sites with an optimal distance are needed. The studies on single Rh crystals suggest that cubic Rh nanoparticles could be a good AZOR electrocatalyst.

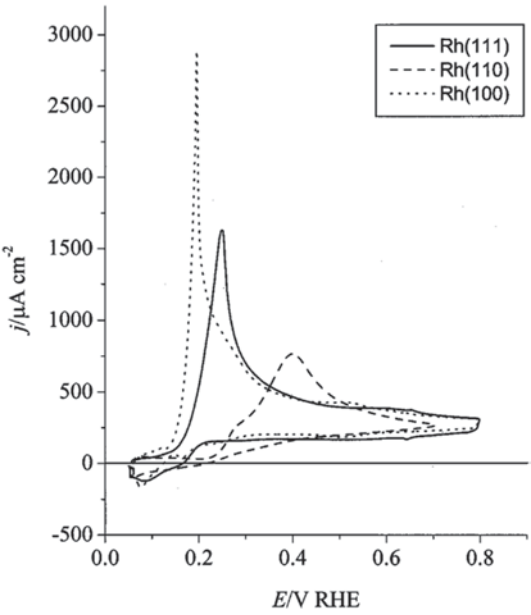

Fig. 7.23 Cyclic voltammetry of HZOR in 0.1 M $HClO_4$ on different Rh single crystal electrodes (reprinted with permission from [118], copyright 2002 Electrochemical Society)

References

1. Peng Z, Yang H (2009) Designer platinum nanoparticles: Control of shape, composition in alloy, nanostructure and electrocatalytic property. Nano Today 4:143–164
2. Chan KY, Ding J, Ren JW et al (2004) Supported mixed metal nanoparticles as electrocatalysts in low temperature fuel cells. J. Mater. Chem. 14:505–516
3. Guo D-J, Ding Y (2012) Porous nanostructured metals for electrocatalysis. Electroanal. 24:2035–2043
4. Kelly TG, Chen JG (2012) Metal overlayer on metal carbide substrate: Unique bimetallic properties for catalysis and electrocatalysis. Chem. Soc. Rev. 41:8021–8034
5. Spendelow JS, Wieckowski A (2004) Noble metal decoration of single crystal platinum surfaces to create well-defined bimetallic electrocatalysts. Phys. Chem. Chem. Phys. 6:5094–5118
6. Chen A, Chatterjee S (2013) Nanomaterials based electrochemical sensors for biomedical applications. Chem. Soc. Rev. 42:5425–5438
7. Bing Y, Liu H, Zhang L et al (2010) Nanostructured Pt-alloy electrocatalysts for PEM fuel cell oxygen reduction reaction. Chem. Soc. Rev. 39:2184–2202
8. Lee K, Zhang JJ, Wang HJ et al (2006) Progress in the synthesis of carbon nanotube- and nanofiber-supported pt electrocatalysts for PEM fuel cell catalysis. J. Appl. Electrochem. 36:507–522
9. Shao Y, Liu J, Wang Y et al (2009) Novel catalyst support materials for PEM fuel cells: Current status and future prospects. J. Mater. Chem. 19:46–59
10. Shao Y, Yin G, Gao Y (2007) Understanding and approaches for the durability issues of Pt-based catalysts for PEM fuel cell. J. Power Sources 171:558–566
11. Zhang J, Xie Z, Zhang J et al (2006) High temperature PEM fuel cells. J. Power Sources 160:872–891
12. Cheng F, Chen J (2012) Metal-air batteries: From oxygen reduction electrochemistry to cathode catalysts. Chem. Soc. Rev. 41:2172–2192

13. Kraytsberg A, Ein-Eli Y (2013) The impact of nano-scaled materials on advanced metal-air battery systems. Nano Energy 2:468–480
14. Lee J-S, Kim ST, Cao R et al (2011) Metal-air batteries with high energy density: Li-air versus Zn-air. Adv. Energy Mater. 1:34–50
15. Rahman MA, Wang X, Wen C (2013) High energy density metal-air batteries: A review. J. Electrochem. Soc. 160:A1759–A1771
16. Diaz-Morales O, Calle-Vallejo F, de Munck C et al (2013) Electrochemical water splitting by gold: Evidence for an oxide decomposition mechanism. Chem. Sci. 4:2334–2343
17. Fujii K, Nakamura S, Sugiyama M et al (2013) Characteristics of hydrogen generation from water splitting by polymer electrolyte electrochemical cell directly connected with concentrated photovoltaic cell. Int. J. Hydrogen Energy 38:14424–14432
18. Lopes T, Andrade L, Ribeiro HA et al (2010) Characterization of photoelectrochemical cells for water splitting by electrochemical impedance spectroscopy. Int. J. Hydrogen Energy 35:11601–11608
19. Bagotsky VS (2006) Fundamentals of electrochemistry. John Wiley & Sons, Pennington, New Jersey
20. Gasteiger HA, Kocha SS, Sompalli B et al (2005) Activity benchmarks and requirements for Pt, Pt-alloy, and non-Pt oxygen reduction catalysts for PEMFCs. Appl. Catal. B-Environ. 56:9–35
21. Marin GB, Yablonsky GS (2011) Kinetics of chemical reactions. Wiley-VCH Verlag & Co., Weinheim
22. Bard AJ, Faulkner LR (2001) Electrochemical methods—fundamentals and applications. John Wiley & Sons, United States
23. Koper MTM, Santen RAv, Neurock M (2003) Theory and modeling of catalytic and electrocatalytic reactions. In: Wieckowski A, Savinova ERVayenas CG (ed) Catalysis and electrocatalysis at nanoparticle surfaces, Marcel Dekker, New York, p 1–34
24. Thomas JM, Thomas WJ (1996) Principles and practice of heterogeneous catalysis. John Wiley & Sons, Weinheim
25. Lima FHB, Zhang J, Shao MH et al (2007) Catalytic activity-d-band center correlation for the O_2 reduction reaction on platinum in alkaline solutions. J. Phys. Chem. C 111:404–410
26. Skoplyak O, Barteau MA, Chen JGG (2006) Reforming of oxygenates for H_2 production: Correlating reactivity of ethylene glycol and ethanol on Pt(111) and Ni/Pt(111) with surface d-band center. J. Phys. Chem. B 110:1686–1694
27. Alonso JA (2000) Electronic and atomic structure, and magnetism of transition-metal clusters. Chem. Rev. 100:637–677
28. Greeley J, Norskov JK, Mavrikakis M (2002) Electronic structure and catalysis on metal surfaces. Annual Rev. Phys. Chem. 53:319–348
29. Low GG (1969) Electronic structure of some transition metal alloys. Adv. Phys. 18:371–&
30. Ruban A, Hammer B, Stoltze P et al (1997) Surface electronic structure and reactivity of transition and noble metals. J. Mol. Catal. A-Chem. 115:421–429
31. Demirci UB (2007) Theoretical means for searching bimetallic alloy as anode electrocatlaysts for direct liquid-feed fuel cells. J. Power Sources 173:11–18
32. Garcia G, Rodriguez P, Rosca V et al (2009) Fourier transform infrared spectroscopy study of CO electro-oxidation on Pt(111) in alkaline media. Langmuir 25:13661–13666
33. Liu Y, Li D, Stamenkovic VR et al (2011) Synthesis of Pt_3Sn alloy nanoparticles and their catalysis for electro-oxidation of CO and methanol. ACS Catal. 1:1719–1723
34. McGrath P, Fojas AM, Reimer JA et al (2009) Electro-oxidation kinetics of adsorbed co on platinum electrocatalysts. Chem. Eng. Sci. 64:4765–4771
35. Zhang C, Hwang SY, Peng Z (2013) Shape-enhanced ammonia electro-oxidation property of a cubic platinum nanocrystal catalyst prepared by surfactant-free synthesis. J. Mater. Chem. A 1:14402–14408
36. Spendelow JS, Babu PK, Wieckowski A (2005) Electrocatalytic oxidation of carbon monoxide and methanol on platinum surfaces decorated with ruthenium. Curr. Opinion Solid State Mater. Sci. 9:37–48

37. Cohen JL, Volpe DJ, Abruna HD (2007) Electrochemical determination of activation energies for methanol oxidation on polycrystalline platinum in acidic and alkaline electrolytes. Phys. Chem. Chem. Phys. 9:49–77
38. Antolini E, Salgado JRC, Gonzalez ER (2006) The methanol oxidation reaction on platinum alloys with the first row transition metals—the case of Pt-Co and -Ni alloy electrocatalysts for DMFCs: A short review. Appl. Catal. B-Environ. 63:137–149
39. Wu J, Yang H (2013) Platinum-based oxygen reduction electrocatalysts. Acc. Chem. Res. 46:1848–1857
40. Wang C, Markovic NM, Stamenkovic VR (2012) Advanced platinum alloy electrocatalysts for the oxygen reduction reaction. ACS Catal. 2:891–898
41. Antolini E, Lopes T, Gonzalez ER (2008) An overview of platinum-based catalysts as methanol-resistant oxygen reduction materials for direct methanol fuel cells. J. Alloys and Compounds 461:253–262
42. Alonso-Vante N (2010) Platinum and non-platinum nanomaterials for the molecular oxygen reduction reaction. ChemPhysChem 11:2732–2744
43. Kim KT, Hwang JT, Kim YG et al (1993) Surface and catalytic properties of iron-platinum carbon electrocatalysts for cathodic oxygen reduction in PAFC. J. Electrochem. Soc. 140:31–36
44. Hwang JT, Chung JS (1993) The morphological and surface-properties and their relationship with oxygen reduction activity for platinum-iron electrocatalysts. Electrochimica Acta 38:2715–2723
45. Tegou A, Papadimitriou S, Armyanov S et al (2008) Oxygen reduction at platinum- and gold-coated iron, cobalt, nickel and lead deposits on glassy carbon substrates. J. Electroanal. Chem. 623:187–196
46. Tegou A, Papadimitriou S, Pavfidou E et al (2007) Oxygen reduction at platinum- and gold-coated copper deposits on glassy carbon substrates. J. Electroanal. Chem. 608:67–77
47. Alia SM, Jensen K, Contreras C et al (2013) Platinum coated copper nanowires and platinum nanotubes as oxygen reduction electrocatalysts. ACS Catal. 3:358–362
48. Spendelow JS, Lu GQ, Kenis PJA et al (2004) Electrooxidation of adsorbed co on Pt(111) and Pt(111)/Ru in alkaline media and comparison with results from acidic media. J. Electroanal. Chem. 568:215–224
49. Peng Z, Yang H (2009) PtAu bimetallic heteronanostructures made by post-synthesis modification of Pt-on-Au nanoparticles. Nano Res. 2:406–415
50. Morimoto Y, Yeager EB (1998) CO oxidation on smooth and high area Pt, Pt-Ru and Pt-Sn electrodes. J. Electroanal. Chem. 441:77–81
51. Calle-Vallejo F, Koper MTM, Bandarenka AS (2013) Tailoring the catalytic activity of electrodes with monolayer amounts of foreign metals. Chem. Soc. Rev. 42:5210–5230
52. Roychowdhury C, Matsumoto F, Zeldovich VB et al (2006) Synthesis, characterization, and electrocatalytic activity of ptbi and ptpb nanoparticles prepared by borohydride reduction in methanol. Chem. Mater. 18:3365–3372
53. Matsumoto F (2012) Ethanol and methanol oxidation activity of PtPb, PtBi, and $PtBi_2$ intermetallic compounds in alkaline media. Electrochem. 80:132–138
54. Tao F, Dag S, Wang L-W et al (2009) Restructuring of hex-Pt(100) under CO gas environments: Formation of 2-D nanoclusters. Nano Lett. 9:2167–2171
55. Yajima T, Uchida H, Watanabe M (2004) In-situ ATR-FTIR spectroscopic study of electrooxidation of methanol and adsorbed co at Pt-Ru alloy. J. Phys. Chem. B 108:2654–2659
56. Radmilovic V, Gasteiger HA, Ross PN (1995) Structure and chemical-composition of a supported Pt-Ru electrocatalyst for methanol oxidation. J. Catal. 154:98–106
57. Iwasita T, Hoster H, John-Anacker A et al (2000) Methanol oxidation on PtRu electrodes. Influence of surface structure and Pt-Ru atom distribution. Langmuir 16:522–529
58. Gojkovic SL, Vidakovic TR, Durovic DR (2003) Kinetic study of methanol oxidation on carbon-supported PtRu electrocatalyst. Electrochimica Acta 48:3607–3614
59. Chu D, Gilman S (1996) Methanol electro-oxidation on unsupported Pt-Ru alloys at different temperatures. J. Electrochem. Soc. 143:1685–1690

60. Gattrell M, MacDougall B (2003) The oxygen reduction/evolution reaction. In: Vielstich W, Lamm AGasteiger HA (ed) Handbook of fuel cells— fundamentals technology and applications, vol. 2: Electrocatalysis, John Wiley & Sons, Chichester, p 443–464
61. Zhang C, Hwang SY, Trout A et al (2014) Solid-state chemistry-enabled scalable production of octahedral Pt–Ni alloy electrocatalyst for oxygen reduction reaction. J. Am. Chem. Soc. 136:7805–7808
62. Stamenkovic VR, Fowler B, Mun BS et al (2007) Improved oxygen reduction activity on $Pt_3Ni(111)$ via increased surface site availability. Science 315:493–497
63. Carpenter MK, Moylan TE, Kukreja RS et al (2012) Solvothermal synthesis of platinum alloy nanoparticles for oxygen reduction electrocatalysis. J. Am. Chem. Soc. 134:8535–8542
64. Lim B, Jiang M, Camargo PHC et al (2009) Pd-Pt bimetallic nanodendrites with high activity for oxygen reduction. Science 324:1302–1305
65. Wang D, Xin HL, Hovden R et al (2013) Structurally ordered intermetallic platinum–cobalt core–shell nanoparticles with enhanced activity and stability as oxygen reduction electrocatalysts. Nature Mater. 12:81–87
66. Wu J, Qi L, You H et al (2012) Icosahedral platinum alloy nanocrystals with enhanced electrocatalytic activities. J. Am. Chem. Soc. 134:11880–11883
67. Hong JW, Kang SW, Choi B-S et al (2012) Controlled synthesis of Pd–Pt alloy hollow nanostructures with enhanced catalytic activities for oxygen reduction. 6:2410–2419
68. Stephens IEL, Bondarenko AS, Perez-Alonso FJ et al (2011) Tuning the activity of Pt(111) for oxygen electroreduction by subsurface alloying. 133:5485–5491
69. Wang JX, Inada H, Wu L et al (2009) Oxygen reduction on well-defined core–shell nanocatalysts: Particle size, facet, and pt shell thickness effects. J. Am. Chem. Soc. 131:17298–17302
70. Zhang J, Lima FHB, Shao MH et al (2005) Platinum monolayer on nonnoble metal–noble metal core–shell nanoparticle electrocatalysts for O_2 reduction. J. Phys. Chem. B 109:22701–22704
71. Zhang Y, Hsieh Y-C, Volkov V et al (2014) High performance Pt monolayer catalysts produced via core-catalyzed coating in ethanol. 738–742
72. Shao M, Shoemaker K, Peles A et al (2010) Pt monolayer on porous Pd–Cu alloys as oxygen reduction electrocatalysts. J. Am. Chem. Soc. 132:9253–9255
73. Zhang L, Iyyamperumal R, Yancey DF et al (2013) Design of Pt-shell nanoparticles with alloy cores for the oxygen reduction reaction. ACS Nano 7:9168–9172
74. Kibsgaard J, Gorlin Y, Chen Z et al (2012) Meso-structured platinum thin films: Active and stable electrocatalysts for the oxygen reduction reaction. J. Am. Chem. Soc. 134:7758–7765
75. Strasser P, Koh S, Anniyev T et al (2010) Lattice-strain control of the activity in dealloyed core–shell fuel cell catalysts. Nature Chem. 2:454–460
76. Debe MK, Schmoeckel AK, Vernstrom GD et al (2006) High voltage stability of nanostructured thin film catalysts for PEM fuel cells. J. Power Sources 161:1002–1011
77. Ross PN (2003) The oxygen reduction/evolution reaction. In: Vielstich W, Lamm AGasteiger HA (ed) Handbook of fuel cells—fundamentals technology and applications, vol. 2: Electrocatalysis, John Wiley & Sons, Chichester, p 465–480
78. Cui C, Gan L, Heggen M et al (2013) Compositional segregation in shaped Pt alloy nanoparticles and their structural behaviour during electrocatalysis. Nature Mater. 12:765–771
79. Choi S-I, Xie S, Shao M et al (2013) Synthesis and characterization of 9 nm Pt–Ni octahedra with a record high activity of 3.3 A/mgPt for the oxygen reduction reaction. Nano Lett. 13:3420–3425
80. Zhang J, Yang H, Fang J et al (2010) Synthesis and oxygen reduction activity of shape-controlled Pt_3Ni nanopolyhedra. Nano Lett. 10:638–644
81. Wu J, Zhang J, Peng Z et al (2010) Truncated octahedral Pt_3Ni oxygen reduction reaction electrocatalysts. J. Am. Chem. Soc. 132:4984–4985
82. Trasatti S (1984) Electrocatalysis in the anodic evolution of oxygen and chlorine. Electrochimica Acta 29:1503–1512
83. Li H, Lee K, Zhang J (2008) Electrocatalytic H_2 oxidation reaction. In: Zhang J (ed) PEM fuel cell electrocatalysts and catalyst layers, Springer, London, p 135–164

84. Gyenge E (2008) Electrocatalytic oxidation of methanol, ethanol and formic acid. In: Zhang J (ed) PEM fuel cell electrocatalysts and catalyst layers, Springer, London, p 165–287
85. Baldauf M, Kolb DM (1996) Formic acid oxidation on ultrathin Pd films on Au(hkl) and Pt(hkl) electrodes. J. Phys. Chem. 100:11375–11381
86. Hoshi N, Kida K, Nakamura M et al (2006) Structural effects of electrochemical oxidation of formic acid on single crystal electrodes of palladium. J. Phys. Chem. B 110:12480–12484
87. Lee H, Habas SE, Somorjai GA et al (2008) Localized Pd overgrowth on cubic Pt nanocrystals for enhanced electrocatalytic oxidation of formic acid. J. Am. Chem. Soc. 130:5406–+
88. Mazumder V, Sun S (2009) Oleylamine-mediated synthesis of Pd nanoparticles for catalytic formic acid oxidation. J. Am. Chem. Soc. 131:4588–+
89. Wang R, Liao S, Ji S (2008) High performance Pd-based catalysts for oxidation of formic acid. J. Power Sources 180:205–208
90. Choi J-H, Jeong K-J, Dong Y et al (2006) Electro-oxidation of methanol and formic acid on PtRu and PtAu for direct liquid fuel cells. J. Power Sources 163:71–75
91. Obradovic MD, Tripkovic AV, Gojkovic SL (2009) The origin of high activity of Pt-Au surfaces in the formic acid oxidation. Electrochimica Acta 55:204–209
92. Zhang S, Shao Y, Liao H-g et al (2011) Graphene decorated with PtAu alloy nanoparticles: Facile synthesis and promising application for formic acid oxidation. Chem. Mater. 23:1079–1081
93. Casado-Rivera E, Gal Z, Angelo ACD et al (2003) Electrocatalytic oxidation of formic acid at an ordered intermetallic PtBi surface. ChemPhysChem 4:193–199
94. Tripkovic AV, Popovic KD, Stevanovic RM et al (2006) Activity of a PtBi alloy in the electrochemical oxidation of formic acid. Electrochem. Comm. 8:1492–1498
95. Alden LR, Han DK, Matsumoto F et al (2006) Intermetallic PtPb nanoparticles prepared by sodium naphthalide reduction of metal-organic precursors: Electrocatalytic oxidation of formic acid. Chem. Mater. 18:5591–5596
96. Matsumoto F, Roychowdhury C, DiSalvo FJ et al (2008) Electrocatalytic activity of ordered intermetallic PtPb nanoparticles prepared by borohydride reduction toward formic acid oxidation. J. Electrochem. Soc. 155:B148–B154
97. Zhang LJ, Wang ZY, Xia DG (2006) Bimetallic PtPb for formic acid electro-oxidation. J. Alloys and Compounds 426:268–271
98. Peng Z, You H, Yang H (2010) An electrochemical approach to PtAg alloy nanostructures rich in Pt at the surface. Adv. Func. Mater. 20:3734–3741
99. Kowal A, Li M, Shao M et al (2009) Ternary Pt/Rh/SnO_2 electrocatalysts for oxidizing ethanol to CO_2. Nature Mater. 8:325–330
100. Cairns EJ, Simons EL, Tevebaug AD (1968) Ammonia-oxygen fuel cell. Nature 217:780–781
101. Rees NV, Compton RG (2011) Carbon-free energy: A review of ammonia- and hydrazine-based electrochemical fuel cells. Energy Environ. Sci. 4:1255–1260
102. Schuth F, Palkovits R, Schlogl R et al (2012) Ammonia as a possible element in an energy infrastructure: Catalysts for ammonia decomposition. Energy Environ. Sci. 5:6278–6289
103. de Mishima BAL, Lescano D, Holgado TM et al (1998) Electrochemical oxidation of ammonia in alkaline solutions: Its application to an amperometric sensor. Electrochim. Acta 43:395–404
104. Diaz LA, Botte GG (2012) Electrochemical deammonification of synthetic swine wastewater. Ind. Eng. Chem. Res. 51:12167–12172
105. Feng C, Sugiura N, Shimada S et al (2003) Development of a high performance electrochemical wastewater treatment system. J. Hazard. Mater. 103:65–78
106. Gerische H, Mauerer A (1970) Studies on anodic oxidation of ammonium on platinum electrodes. J. Electroanal. Chem. 25:421–433
107. Rosca V, Duca M, de Groot MT et al (2009) Nitrogen cycle electrocatalysis. Chem. Rev. 109:2209–2244
108. Gootzen JFE, Wonders AH, Visscher W et al (1998) A DEMS and cyclic voltammetry study of NH_3 oxidation on platinized platinum. Electrochim. Acta 43:1851–1861

109. de Vooys ACA, Mrozek MF, Koper MTM et al (2001) The nature of chemisorbates formed from ammonia on gold and palladium electrodes as discerned from surface-enhanced Raman spectroscopy. Electrochem. Commun. 3:293–298
110. Endo K, Katayama Y, Miura T (2005) A rotating disk electrode study on the ammonia oxidation. Electrochim. Acta 50:2181–2185
111. Vidal-Iglesias FJ, Solla-Gullon J, Montiel V et al (2005) Ammonia selective oxidation on pt(100) sites in an alkaline medium. J. Phys. Chem. B 109:12914–12919
112. Rosca V, Koper MTM (2006) Electrocatalytic oxidation of ammonia on pt(111) and pt(100) surfaces. Phys. Chem. Chem. Phys. 8:2513–2524
113. Vidal-Iglesias FJ, García-Aráez N, Montiel V et al (2003) Selective electrocatalysis of ammonia oxidation on pt(100) sites in alkaline medium. 5:22–26
114. Novell-Leruth G, Valcarcel A, Clotet A et al (2005) DFT characterization of adsorbed NHx species on Pt(100) and Pt(111) surfaces. J. Phys. Chem. B 109:18061–18069
115. Novell-Leruth G, Ricart JM, Perez-Ramirez J (2008) Pt(100)-catalyzed ammonia oxidation studied by DFT: Mechanism and microkinetics. J. Phys. Chem. C 112:13554–13562
116. Novell-Leruth G, Valcarcel A, Perez-Ramirez J et al (2007) Ammonia dehydrogenation over platinum-group metal surfaces. Structure, stability, and reactivity of adsorbed NHx species. J. Phys. Chem. C 111:860–868
117. Offermans WK, Jansen APJ, van Santen RA et al (2007) Ammonia dissociation on Pt{100}, Pt{111}, and Pt{211}: A comparative density functional theory study. J. Phys. Chem. C 111:17551–17557
118. Alvarez-Ruiz B, Gomez R, Orts JM et al (2002) Role of the metal and surface structure in the electro-oxidation of hydrazine in acidic media. J. Electrochem. Soc. 149:D35–D45